REPORT 1274

SECOND-ORDER SUBSONIC AIRFOIL THEORY INCLUDING EDGE EFFECTS [1]

By Milton D. Van Dyke

SUMMARY

Several recent advances in plane subsonic flow theory are combined into a unified second-order theory for airfoil sections of arbitrary shape. The solution is reached in three steps: The incompressible result is found by integration, it is converted into the corresponding subsonic compressible result by means of the second-order compressibility rule, and it is rendered uniformly valid near stagnation points by further rules. Solutions for a number of airfoils are given and are compared with the results of other theories and of experiment. A straight-forward computing scheme is outlined for calculating the surface velocities and pressures on any airfoil at any angle of attack.

INTRODUCTION

Thin-airfoil theory provides a useful first approximation to the incompressible flow past two-dimensional airfoils, and the results can be immediately extended to subsonic compressible flow by the Prandtl-Glauert rule. It is natural to attempt to improve this simple theory by successive approximations so as to increase its accuracy for thicker airfoils and higher subsonic Mach numbers. There results a series expansion of the flow quantities in powers (supplemented by logarithms in the fourth and higher approximations) of the airfoil thickness ratio, camber ratio, and angle of attack.

For incompressible flow, the higher-order theory has been studied by various writers, in particular Riegels and Wittich (refs. 1 and 2) and Keune (ref. 3). A less straightforward series of approximations was developed by Goldstein (ref. 4). Perhaps the most concise exposition of higher-order incompressible thin-airfoil theory is given by Lighthill (ref. 5).

For subsonic compressible flow, the corresponding analysis was first undertaken by Görtler (ref. 6), followed by Hantzsche and Wendt (refs. 7 and 8), Schmieden and Kawalki (ref. 9), Kaplan (refs. 10 and 11), Imai and Oyama (refs. 12 and 13) and others. These investigators treated only specific simple shapes by rather laborious analysis. Later, it was discovered that particular integrals of the second-order iteration equation can be expressed in terms of the first approximation (refs. 14 and 15). This permits the second-order subsonic solution for any profile to be given in terms of integrals (refs. 15 and 16). However, the resulting solutions are sometimes incorrect everywhere for airfoils with stagnation points, for reasons to be discussed later.

Recently Hayes (ref. 17), improving on a result of Imai (ref. 18), has given a second-order similarity rule for surface pressure that implies a second-order extension of the Prandtl-Glauert rule (ref. 19). This remarkable result was overlooked by earlier investigators because they did not calculate surface pressures, but were content with finding surface speeds, for which the second-order compressibility rule is more complicated. These rules reduce the second-order problem of subsonic compressible flow past airfoils to the corresponding incompressible problem.

However, the solution by successive approximations breaks down near leading and trailing edges if there are stagnation points. The result is therefore merely a formal series expansion, which fails to converge near the edges. In first-order theory spurious singularities arise at stagnation edges, but it is known how they can be taken into account, since they are integrable. In the second approximation, however, these singularities are intensified, so that at round edges they are no longer integrable. In any case, the calculated speeds and pressures are incorrect near such edges, and more so in the second approximation than the first. Moreover, in subsonic compressible flow the second approximation may be incorrect everywhere as a consequence of the defects in the first approximation.

For round edges in incompressible flow, previous investigators have shown how these defects can be corrected. Riegels (ref. 2) gave a simple rule that renders the first-order thin-airfoil solution valid near the edge. Lighthill (ref. 5) gave an equivalent rule for the second approximation. Recently, corresponding rules have been developed for higher approximations, for sharp as well as round edges, and for subsonic compressible flow (ref. 20).

It is the aim of this paper to combine these recent advances into a unified theory. There results a uniform second approximation to subsonic flow past any profile at angle of attack, expressed in terms of integrals that can, if necessary, be evaluated numerically. It may be noted that, except possibly for certain particular shapes at isolated Mach numbers, the resulting solution is now generally believed to be valid only below the critical Mach number—that is, for purely subsonic flows. Although only flow quantities at the airfoil surface are considered here in detail, the entire flow field could be treated in the same way.

For numerical computation, the most useful method appears to be that initiated by Riegels and Wittich (refs. 1 and 2) and independently by Germain (ref. 21), with

extensions by Watson (ref. 22), Thwaites (ref. 23), and Weber (ref. 24 and 25). It requires a knowledge only of the airfoil ordinates at a specified set of points. In this report a straightforward scheme, based on an extension of this method, is given for computing the second-order subsonic solution for any airfoil. The reader interested only in calculating a specific case, without necessarily understanding the details of the theory, can turn directly to the section "PRACTICAL NUMERICAL COMPUTATION."

The author is indebted to R. T. Jones for many helpful discussions throughout the course of this work.

THEORY

From the preceding remarks it is clear that the solution is reached in three steps. First, the formal second-order incompressible solution is found by integration. Second, this is converted into the corresponding subsonic compressible solution by means of the second-order compressibility rule. Third, this is modified near stagnation points by the appropriate rules for round or sharp edges. These three steps will be considered successively.

FORMAL INCOMPRESSIBLE SOLUTION

The expansion of the velocity components in a formal series of powers of the airfoil thickness ratio, camber ratio, and angle of attack has been discussed in detail by Lighthill (ref. 5). It will suffice here to summarize his results for the second approximation. We mainly follow his notation except to make it more mnemonic, and to suppress his parameter ϵ characteristic of the airfoil thickness, which is only convenient in the detailed analysis.

Accordingly, consider an airfoil of moderate thickness and camber at a moderate angle of attack to a uniform subsonic stream (fig. 1). It is essential that the x axis be chosen to pass through both the leading and trailing edges. Let the upper and lower surfaces of the airfoil be described by
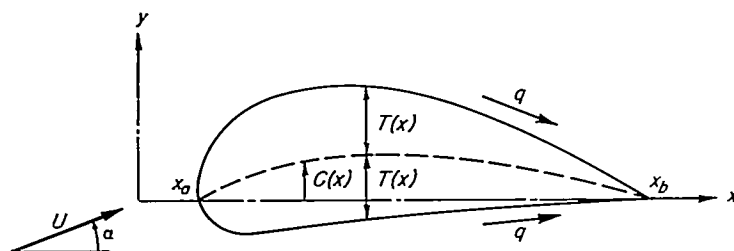
$$y=Y(x)=C(x)\pm T(x) \tag{1}$$

FIGURE 1.—Notation for airfoil.

where $C(x)$ describes the mean camber line and $T(x)$ the thickness. The airfoil extends over the interval $x_a \leq x \leq x_b$, which is usually conveniently taken to be either $-1 \leq x \leq 1$ or $0 \leq x \leq 1$. All symbols are defined in Appendix A.

First-order solution.—In the first approximation of thin-airfoil theory, the condition of tangent flow at the airfoil surface is imposed on the two sides of the chord line $y=0$ rather than at the surface, and requires that

$$\frac{v_1}{U}\bigg|_{y=0}=Y'(x)=C'(x)\pm T'(x) \tag{2}$$

The corresponding horizontal velocity disturbance on the chord line, which is required for calculating the surface pressure, consists of a term associated with the airfoil thickness, and another associated with its camber and angle of attack. For the thickness

$$\frac{u_{1t}}{U}=\frac{1}{\pi}\oint_{x_a}^{x_b}\frac{T'(\xi)d\xi}{x-\xi} \tag{3}$$

and for the camber and angle of attack

$$\frac{u_{1c}}{U}=\left(\frac{x_b-x}{x-x_a}\right)^{1/2}\left[\alpha+\frac{1}{\pi}\oint_{x_a}^{x_b}\left(\frac{\xi-x_a}{x_b-\xi}\right)^{1/2}\frac{C'(\xi)d\xi}{x-\xi}\right] \tag{4}$$

The latter result is due to Munk (ref. 26) and the former was first given by Pistolesi (ref. 27). Cauchy principal values are indicated in each integral.

The surface speed is then given to a first approximation by

$$\frac{q_1}{U}=1+\frac{u_{1t}}{U}\pm\frac{u_{1c}}{U} \tag{5}$$

Second-order solution.—In the second approximation, the tangency condition is transferred from the airfoil surface to the chord line by Taylor series expansion. The condition on the second-order increment in vertical velocity is thus found to be

$$\frac{v_2}{U}\bigg|_{y=0}=C'_2(x)\pm T'_2(x) \tag{6a}$$

where

$$\left.\begin{array}{l}C_2(x)=\dfrac{u_{1t}}{U}\,C+\dfrac{u_{1c}}{U}\,T \\[2mm] T_2(x)=\dfrac{u_{1t}}{U}\,T+\dfrac{u_{1c}}{U}\,C\end{array}\right\} \tag{6b}$$

(We depart here from Lighthill's notation in order to emphasize that the functions C_2 and T_2 are effectively the camber and thickness for some fictitious airfoil.) The problem is identical with that in first-order theory except for the condition at infinity, which is readily disposed of. Thus, corresponding to T_2 is the increment in horizontal velocity

$$\frac{u_{2t}}{U}=\frac{1}{\pi}\oint_{x_a}^{x_b}\frac{T'_2(\xi)d\xi}{x-\xi}-\frac{1}{2}\alpha^2 \tag{7}$$

and corresponding to C_2

$$\frac{u_{2c}}{U}=\frac{1}{\pi}\left(\frac{x_b-x}{x-x_a}\right)^{1/2}\oint_{x_a}^{x_b}\left(\frac{\xi-x_a}{x_b-\xi}\right)^{1/2}\frac{C'_2(\xi)d\xi}{x-\xi} \tag{8}$$

The velocity components on the surface of the airfoil include also terms arising from the transfer from the chord line to the surface, which is again effected by Taylor series expansion. Hence the surface speed is given to a second approximation by

$$\frac{q_2}{U}=1+\frac{u_{1t}}{U}\pm\frac{u_{1c}}{U}+\frac{u_{2t}}{U}\pm\frac{u_{2c}}{U}+(C\pm T)(C''\pm T'')+\frac{1}{2}(C'\pm T')^2 \tag{9}$$

and the surface pressure coefficient by

$$C_{p2}=-2\left(\frac{q_2}{U}-1\right)-\left(\frac{u_{1t}}{U}\pm\frac{u_{1c}}{U}\right)^2 \tag{10}$$

Higher-order solutions can be found by continuing this process. Lighthill gives explicit formulas for the third-order solution.

Airfoil integrals.—The incompressible solution to second order (or, indeed, to any order) is thus reduced to a succession of "airfoil integrals" typified by equations (3), (4), (7), and (8). Goldstein (ref. 28) emphasizes that in first-order theory these integrals can be evaluated analytically for practically every profile for which formulas have ever been proposed. In second-order theory this appears to true to a somewhat lesser extent, although the labor of calculation becomes great except for simple shapes. Often the integrals are most readily evaluated by guessing $(u-iv)$ as a function of the complex variable $(x+iy)$ that has the required behavior on the chord line. A short table of airfoil integrals useful for finding second-order solutions is given in Appendix B. Other can be found in references 28, 29, and 30.

For complicated profiles, exact analytic evaluation of the integrals may be impossible or excessively laborious. Then numerical integration may be resorted to, or the profile can be approximated by a simpler shape that can be treated analytically. The most useful numerical procedure is apparently that originated independently by Riegels and Germain and simplified and extended by Watson, Thwaites, and Weber. In this method the airfoil ordinates are approximated by the trigonometric polynomial

$$Y \approx k_0 + \sum_{r=1}^{N-1} (k_r \cos r\theta + t_r \sin r\theta) + k_N \cos N\theta$$
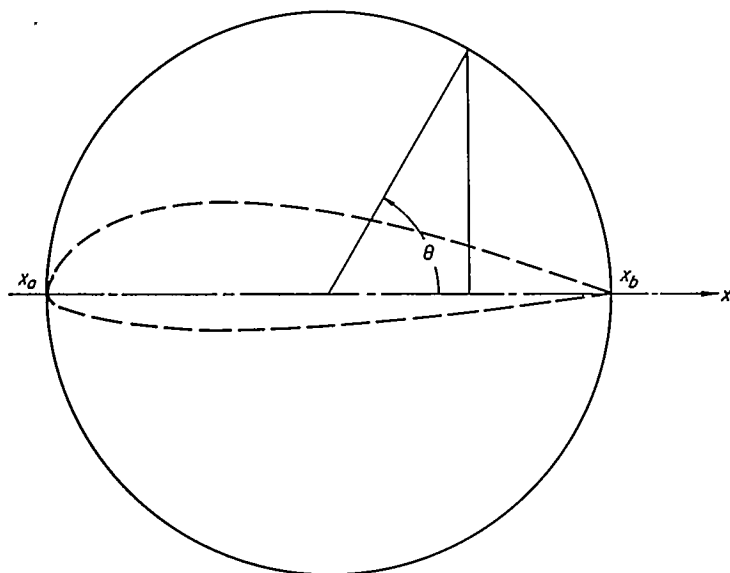

FIGURE 2.—Parametric angle θ.

where θ is the angle indicated in figure 2. The coefficients k_r (for camber) and t_r (for thickness) are chosen to give the actual ordinates at the $2N$ points for which $\theta = m\pi/N$. In this way it is found that the airfoil integrals can be expressed approximately as sums of the airfoil ordinates at certain pivotal points multiplied by standard influence coefficients. The details of this method, as adapted to second-order thin-airfoil theory, are given in Appendix C. The numerical computing procedure is outlined in the last section of this paper.

SECOND-ORDER COMPRESSIBILITY RULE

The second-order counterpart of the Prandtl-Glauert compressibility rule is implicit in an extension of transonic similitude that was initiated by Imai (ref. 18) and carried to completion by Hayes (ref. 17). Imai sought to improve the transonic similarity rule by retaining in its derivation all terms proportional to the square of the airfoil thickness except one appearing in the condition of tangent flow at the surface. The correlation of experimental data was not appreciably improved, which led him to suggest that the neglected second-power term should also be included. This probably cannot be done for the whole flow field. However, in attempting merely to reproduce Imai's result as announced before publication, Hayes actually included that term in a second-order rule for surface pressure.

Hayes' result is that for two-dimensional subsonic or supersonic flow the ratio of the second-order to first-order pressure term on the surface is proportional to the parameter

$$\frac{\tau}{(|1-M^2|)^{3/2}} \left[\frac{\gamma+1}{2} M^4 + 2(1-M^2) \right] \qquad (11)$$

where τ is some measure of the thickness, camber, or angle of attack. Now at subsonic speeds the first-order pressure term is related to its value in incompressible flow by the Prandtl-Glauert rule. Combining these two results yields the second-order compressibility rule (ref. 19).

In incompressible flow the second-order surface-pressure coefficient has the form

$$C_{p_0}(x) = C_{p_1}(x) + \Delta C_{p_2}(x) \qquad (12a)$$

where the first-order term C_{p_1} contains linear terms in thickness, camber, and angle of attack, and the second-order increment ΔC_{p_2} contains their squares and products. Then for the same airfoil in subsonic compressible flow, according to the compressibility rule, the pressure coefficient is

$$C_{p_M} = K_1 C_{p_1} + K_2 (\Delta C_{p_2}) \qquad (12b)$$

where

$$\left. \begin{aligned} K_1 &= \frac{1}{\sqrt{1-M^2}} = \frac{1}{\beta} \\[2mm] K_2 &= \frac{(\gamma+1)M^4 + 4\beta^2}{4\beta^4} \end{aligned} \right\} \qquad (12c)$$

The corresponding compressibility rule for surface speed is readily found from the above rule for pressure by considering the small-disturbance series form of Bernoulli's equation for compressible flow. Thus it is found that if the surface speed ratio in incompressible flow is

$$\frac{q_0}{U} = 1 + \frac{\Delta q_1}{U} + \frac{\Delta q_2}{U} \qquad (13a)$$

where Δq_1 contains linear terms in thickness, camber, and angle of attack, and Δq_2 their squares and products, then at subsonic speeds

$$\frac{q_M}{U} = 1 + K_1 \frac{\Delta q_1}{U} + K_2 \frac{\Delta q_2}{U} + \frac{K_2-1}{2} \left(\frac{\Delta q_1}{U} \right)^2 \qquad (13b)$$

with

$$\frac{K_2-1}{2}=M^2\frac{(\gamma+1)M^2+4\beta^2}{8\beta^4} \qquad (13c)$$

This rule is seen to lack the fundamental simplicity of the rule for pressure.

EDGE CORRECTIONS

Thin-airfoil theory is known to fail near leading and trailing edges if there is a stagnation point. The flow is actually brought to rest, but thin-airfoil theory predicts infinite speeds instead. If r is the distance from the edge, the velocity contains powers of $r^{-1/2}$ for a round edge and for any leading edge with flow around it (associated with angle of attack), and powers of $\ln r$ for a sharp edge. First-order theory contains first powers of these singularities, second-order theory their squares and products, and so on, so that the formal thin-airfoil series diverges in some neighborhood of the edge. Not only are the velocities and pressure incorrect near stagnation edges, but nonintegrable singularities appear in the higher-order expressions for aerodyanmic forces on round edges.

False subsonic solutions.—Even more serious difficulties may arise in subsonic compressible flow, where the infection spreads in some cases so that the formal second-order solution is incorrect not only near the edges but over the entire airfoil surface. Thus, using the particular integral of reference 14, Harder and Klunker gave an expression for the second-order solution for any symmetric airfoil at zero angle of attack (ref. 16). However, they noted that their expression does not apply to round-edged airfoils, for which it contains divergent integrals. A more deceptive defect appears if their expression is applied to a sharp-edged airfoil such as a biconvex section; then the predicted surface speeds are finite (except near the edges) but incorrect everywhere by a term proportional to M^2. This defect arises from the fact that near sharp edges the first-order source distribution is not approximately the airfoil slope, as is assumed in thin-airfoil theory. The second-order solution involves the derivative of the source strength which, as indicated in figure 3, has infinite peaks that are missed by thin-airfoil

FIGURE 3.—Source strength for biconvex airfoil.

theory. It is enough to take account of this shortcoming in even the crudest fashion. Thus, if the region of integration is extended an infinitesimal distance beyond the edges to include the pulses (Dirac delta functions) of the thin-airfoil approximation, Harder and Klunker's expression yields a solution that is correct to second order except in the vicinity of the edges.

Keune has discovered an alternative particular integral containing the stream function rather than the velocity potential, and so has obtained another expression for the second-order solution (ref. 15). Because the tangency condition is one degree smoother for the stream function than the velocity potential, his expression yields the correct result (except near stagnation edges) for sharp-edged shapes. It fails, however, for round-edged shapes, so that his solution for subsonic flow past an ellipse is incorrect everywhere.

Both these expressions can be manipulated by partial integration so as to be correct except near stagnation edges. However, the result is simply that obtained by applying the second-order compressibility rule to the expressions for second-order incompressible flow. Hence these more serious difficulties are of no further concern here. They do serve, however, to warn of the danger of false second-order solutions in more complicated problems.

The role of edge corrections.—Thin-airfoil theory fails near stagnation edges because there the basic assumption of small disturbances is violated. It might be feared that uniformly valid solutions could be found only by abandoning that assumption, which leads to such great mathematical simplification. Fortunately, however, Riegels and Lighthill have shown that for round edges in incompressible flow all the results of small-disturbance theory can be salvaged. They have given simple rules to be applied to the formal thin-airfoil solution that render it uniformly valid near the edge.

For present purposes, corresponding rules are required for subsonic as well as incompressible flows, for sharp as well as round edges, and for cambered round edges, for which Lighthill's rule is correct only to first order. It is believed that neither Riegels' nor Lighthill's technique can be extended to these cases. Instead, a different technique is used here, which is particularly suited to the study of edges. It consists in comparing the exact and thin-airfoil solutions for simple shapes that approximate the airfoil in the vicinity of the edge. This technique was first applied in reference 20 to the surface velocity on airfoil sections, three-dimensional wings, and bodies of revolution. It is reproduced here insofar as it applies to second-order theory for airfoil sections, and is extended to treat surface pressures as well as velocities.

Round edges in incompressible flow.—Most subsonic airfoil sections have finite leading-edge radius, and many are actually analytic (except at the training edge). This means that all derivatives are continuous, so that, with s the abscissa measured from the edge into the airfoil, the upper and lower surfaces are described by

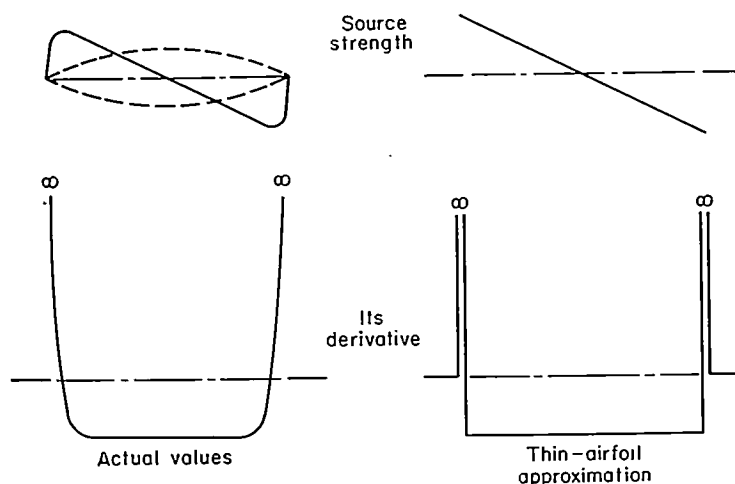$$y=\pm T_0 s^{1/2}+C_1 s\pm T_1 s^{3/2}+C_2 s^2+ \ldots \qquad (14)$$

Here the T_n and C_n are coefficients for the thickness and camber, respectively (fig. 1). Thus T_0 determines the nose radius, C_1 the initial camber, and so on.

Thin-airfoil theory breaks down close to the edge where s is of the order of the leading-edge radius ρ. Now ρ is proportional to the square of the thickness ratio τ, so that thin-airfoil theory fails where $s = 0(\tau^2)$. In this small region the airfoil is described to second order by the first two terms of equation (14). In terms of the leading-edge radius ρ and initial slope λ of the camber line, the airfoil is given by

$$y = \pm\sqrt{2\rho s} + \lambda s \tag{15a}$$

This is the equation of an inclined parabola, described in rotated coordinates by

$$\tilde{y} = \pm\sqrt{2\tilde{\rho}\tilde{s}} \tag{15b}$$

where the two origins of coordinates are separated by a negligible distance, and the difference between ρ and $\tilde{\rho}$ can also be ignored.
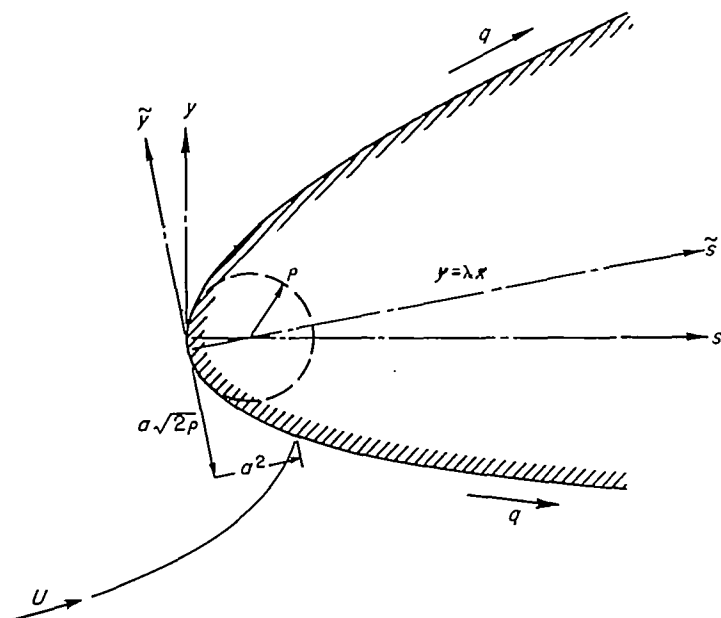

FIGURE 4.—Flow past inclined parabola.

The exact velocity on this parabola in a uniform stream is found, from conformal mapping or otherwise, to be given by

$$\frac{q}{U} = \left(\frac{\tilde{s}}{\tilde{s} + \rho/2}\right)^{1/2}\left(1 \pm \frac{a}{\sqrt{\tilde{s}}}\right) \tag{16}$$

where the signs refer to the upper and lower surfaces. Here a has the physical interpretation that the stagnation point lies at $\tilde{s} = a^2$ and $\tilde{y} = -a\sqrt{2\rho}$ (fig. 4). When the flow past the parabola is related to that near an airfoil nose, a is some moderate multiple of the angle of attack measured from the "ideal" angle—the angle at which the stagnation point coincides with the vertex. The factor of proportionality depends on the entire airfoil shape (and the trailing-edge condition), but its value is not required here. Expanding this expression for small $\rho/\tilde{s}$ yields, to second order, the formal series

$$\frac{q_2}{U} = 1 \pm \frac{a}{\sqrt{\tilde{s}}} - \frac{\rho}{4\tilde{s}} + \ldots \tag{17}$$

and, as it must be, this is the second-order thin-airfoil solution for a parabola. It is clear from this formal expansion how the singularity arises at the leading edge.

The ratio of the exact speed on the parabola to its formal series expansion serves as a multiplicative correction factor for other shapes having the same nose radius. Thus the second-order thin-airfoil solution q_2 for any airfoil of leading-edge radius ρ is converted into an approximation $\bar{q}$ that is uniformily valid near the edge by

$$\frac{\bar{q}}{U} = \frac{\left(\dfrac{\tilde{s}}{\tilde{s} + \rho/2}\right)^{1/2}\left(1 \pm \dfrac{a}{\sqrt{\tilde{s}}}\right)}{1 \pm \dfrac{a}{\sqrt{\tilde{s}}} - \dfrac{\rho}{4\tilde{s}}}\frac{q_2}{U} \tag{18}$$

Simplifying this insofar as possible without destroying its validity near the edge, and retaining only second-order terms, gives the rule

$$\frac{\bar{q}}{U} = \left(\frac{\tilde{s}}{\tilde{s} + \rho/2}\right)^{1/2}\left(\frac{q_2}{U} + \frac{\rho}{4s}\right) \tag{19}$$

It might be supposed that since the airfoil nose was fitted to second order, this rule yields a solution that is uniformly valid to second order. Comparison with various exact solutions indicates that this is true, in the sense that the velocity disturbance and hence the pressure coefficient are correct to second order everywhere (except near the trailing edge, where additional modification is required). This will be indicated by replacing $\bar{q}$ by $\bar{q}_2$.

The oblique abscissa $\tilde{s}$ can be expressed in terms of the original abscissa s, since on the surface of the parabola

$$\tilde{s} = s \pm \lambda\sqrt{2\rho s} + \ldots \tag{20}$$

Hence the rule becomes finally

$$\frac{\bar{q}_2}{U} = \left(\frac{s \pm \lambda\sqrt{2\rho s}}{s \pm \lambda\sqrt{2\rho s} + \rho/2}\right)^{1/2}\left(\frac{q_2}{U} + \frac{\rho}{4s}\right) \tag{21}$$

In the special case $\lambda = 0$ this reduces to Lighthill's rule (ref. 5).

The corresponding rule for surface pressure coefficient is found by proceeding in the same way with the exact pressure on the parabola, which is found from equation (16) using Bernoulli's equation. Again expanding formally for small ρ/s and taking the ratio as a multiplicative correction factor yields the rule

$$\bar{C}_{p_2} = \frac{s \pm \lambda\sqrt{2\rho s}}{s \pm \lambda\sqrt{2\rho s} + \rho/2}C_{p_2} \tag{22}$$

Airfoils of the NACA four- and five-digit series are not analytic at the nose. Their thickness distribution $T(x)$ consists initially of the ordinates of a parabola minus those of a wedge, so that the airfoil is described by

$$y = \pm T_0 s^{1/2} + C_1 s \mp T_1|s| + \ldots \tag{23}$$

These airfoils are fitted only to first order by an inclined parabola, and it follows that the preceding rules render the thin-airfoil solution uniformly valid only to first order near the

edge, though it remains correct to second order elsewhere. An appropriate second-order rule would require finding the conformal mapping for a parabola minus a wedge.

First-order theory; Riegels' rules.—In the first-order theory, the terms in λ can be neglected, so that the rule for pressure, equation (22), simplifies to

$$\overline{C}_{p_1}=\frac{s}{s+\rho/2}\,C_{p_1} \tag{24}$$

The last term in equation (21) is also of second order, so that the rule for speed becomes

$$\frac{\overline{q}_1}{U}=\left(\frac{s}{s+\rho/2}\right)^{\frac{1}{2}}\frac{q_1}{U} \tag{25}$$

This is not precisely Riegels' rule. However, for a parabola

$$\left(\frac{s}{s+\rho/2}\right)^{\frac{1}{2}}=\cos\eta \tag{26}$$

where η is the angle of the surface. Hence an alternative form of equation (25) is

$$\frac{\overline{q}_1}{U}=\cos\eta\,\frac{q_1}{U} \tag{27}$$

and this is Riegels' rule (ref. 2). The corresponding rule for pressure is

$$\overline{C}_{p_1}=(\cos\eta)^2 C_{p_1} \tag{28}$$

These alternative forms suffer the defect of falsely implying that the nose exerts an influence even at remote points if the local airfoil slope is appreciable (for example, at the trailing edge). To this extent they fail to render the solution uniformly valid. However, it happens that they are exact for ellipses as well as parabolas, and are accordingly much more accurate for most airfoils, as indicated by the example of figure 5.
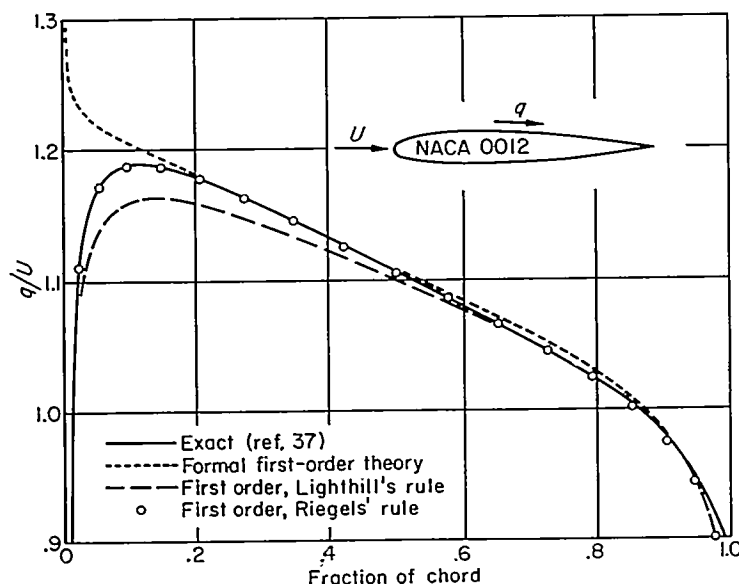

FIGURE 5.—Comparison of Lighthill's and Riegels' rules for incompressible flow past NACA 0012 airfoil.

The second-order rules can be manipulated into the form of Riegels' rule (ref. 20), but the slight advantages of accuracy and simplicity then scarcely offset their defects. The same is true of the rules for compressible flow given later. Hence Riegels' rules are recommended only for first-order incompressible-flow theory.

Round edges in subsonic flow.—The previous rules can be extended to subsonic speeds simply by considering subsonic rather than incompressible flow past an inclined parabola. Although no exact solution of this problem is known, existing approximate solutions by the Janzen-Rayleigh method are probably sufficiently accurate, at least at the ideal angle of attack, and could, in principle be refined indefinitely. Alternatively, one could use experimental measurements on a parabola.

The problem is defined by ρ and a and the free-stream Mach number M. (The adiabatic exponent γ also enters, but is assumed fixed at 7/5.) Therefore, dimensional reasoning shows that the surface speed is given by

$$\frac{q}{U}=Q\left(\frac{\tilde{s}}{\rho/2},\pm\frac{a}{\sqrt{\rho/2}},M\right) \tag{29}$$

where, as usual, the upper and lower signs apply to the upper and lower surfaces. (Choosing $\rho/2$ rather than ρ as the reference length leads to later simplification.) Expanding this function formally for x large compared with ρ and a^2 would yield the thin-airfoil series, which is, to second order

$$\frac{q_2}{U}=1\pm K_1\frac{a}{\sqrt{\tilde{s}}}-K_2\frac{\rho}{4\tilde{s}}+\frac{K_2-1}{2}\frac{a^2}{\tilde{s}} \tag{30}$$

where K_1 and K_2 are the compressibility factors of equation (12c). Again the ratio of Q to its series expansion serves as a multiplicative correction factor to be applied to any round-nosed airfoil. Simplifying as before, and replacing $\tilde{s}$ by s according to equation (20), gives the rule[2]

$$\frac{\overline{q}_2}{U}=Q\left(\frac{s\pm\lambda\sqrt{2\rho s}}{\rho/2},\pm\frac{a}{\sqrt{\rho/2}},M\right)\times$$

$$\left[\frac{q_2}{U}\mp K_1\frac{a}{\sqrt{s}}\frac{q_1}{U}+\frac{K_2}{4}\frac{\rho}{s}+\left(K_1^2-\frac{K_2-1}{2}\right)\frac{a^2}{s}\right] \tag{31}$$

where q_1/U is the first-order thin-airfoil solution. Here a must be identified as the coefficient of $\pm K_1/\sqrt{s}$ in the second-order solution, as is clear from equation (30). (The physical interpretation of a shown in fig. 4 is valid only at zero Mach number.)

The corresponding rule for pressure is found by considering the exact pressure coefficient for the parabola, which must have the form

$$C_p=\Pi\left(\frac{\tilde{s}}{\rho/2},\pm\frac{a}{\sqrt{\rho/2}},M\right) \tag{32}$$

---

[2] As $M\to0$ this reduces not to the rule given previously for incompressible flow, but to an alternative that is equivalent up to terms of second order. The difference arises from the fact that in the incompressible case the dependence of q/U upon a is given explicitly by the factor $(1\pm a/\sqrt{s})$ in equation (16), which is used to cancel a corresponding term in the denominator of equation (18).

Its series expansion would give the thin-airfoil result

$$C_{p2} = \mp 2K_1 \frac{a}{\sqrt{8}} + K_2 \left(\frac{\rho}{28} - \frac{a^2}{8} \right) \qquad (33)$$

Hence the rule for any airfoil is

$$\overline{C}_{p2} = P \left(\frac{8 \pm \lambda \sqrt{2\rho 8}}{\rho/2}, \pm \frac{a}{\sqrt{\rho/2}}, M \right) C_{p2} \qquad (34a)$$

where

$$P \left(\frac{8}{\rho/2}, \pm \frac{a}{\sqrt{\rho/2}}, M \right) = \frac{\Pi \left(\frac{8}{\rho/2}, \pm \frac{a}{\sqrt{\rho/2}}, M \right)}{\mp 2K_1 \frac{a}{\sqrt{8}} + K_2 \left(\frac{\rho}{28} - \frac{a^2}{8} \right)} \qquad (34b)$$

In this case a is the coefficient of $\mp 2K_1/\sqrt{8}$ in the second-order pressure coefficient.

Imai has recently calculated the Janzen-Rayleigh solution for a parabola at the ideal angle of attack including terms in M^4 (ref. 31). Thus, his results give

$$Q \left(\frac{8}{\rho/2}, 0, M \right) = q_0 + M^2 q_1 + M^4 q_2 + 0(M^6) \qquad (35)$$

where the q_n are increasingly complicated functions of $8/(\rho/2)$. In reference 20 an attempt was made to increase the accuracy of this approximation by modifying it so that for large $8/(\rho/2)$ it tends exactly to the second-order thin-airfoil solution of equation (30). However, the third-order thin-airfoil solution has since been calculated by Kaplan (ref. 32):

$$\frac{q_3}{U} = 1 - \frac{1}{2} K_2 \left(\frac{\rho}{28} \right) + \frac{1}{2} K_3 \left[\left(\frac{\rho}{28} \right)^{3/2} + \right.$$

$$\left. \frac{4\beta}{\pi} \left(\frac{\rho}{28} \right)^2 \ln \left(2\beta \sqrt{\frac{\rho}{28}} \right) \right] + 0 \left(\frac{\rho}{28} \right)^2$$

where

$$K_3 = \frac{\pi}{2} \frac{M^2}{\beta^3} \left[1 + \frac{\gamma+1}{8} \frac{M^2}{\beta^2} \left(1 + \frac{\gamma+1}{4} \frac{M^2}{\beta^2} \right) (8-M^2) \right]$$

(It is a matter of taste whether the logarithmic term included here is regarded as being of third or fourth order.) The comparison with this result shown in figure 6 suggests that the modification was detrimental, and that Imai's solution is adequate for practical purposes.[3] A short table of the function $Q[8/(\rho/2), 0, M]$ calculated from equation (35) is given below:

$$Q \left(\frac{8}{\rho/2}, 0, M \right)$$

M \ $8/(\rho/2)$	0	0.5	1	2	4	10	20	50
0	0	0.5774	0.7071	0.8165	0.8944	0.9535	0.9759	0.9901
.4	0	.5570	.6874	.8002	.8829	.9473	.9724	.9885
.5	0	.5449	.6752	.7898	.8753	.9431	.9699	.9874
.6	0	.5295	.6592	.7758	.8648	.9371	.9664	.9858
.7	0	.5104	.6388	.7574	.8508	.9290	.9616	.9835
.8	0	.4870	.6133	.7338	.8324	.9182	.9551	.9805
.85	0	.4737	.5982	.7197	.8213	.9116	.9512	.9788
.9	0	.4590	.5816	.7039	.8088	.9042	.9466	.9765

[3] The table on p. 11 of ref. 20 also involves an error in computing the q_2 of eq. (35).
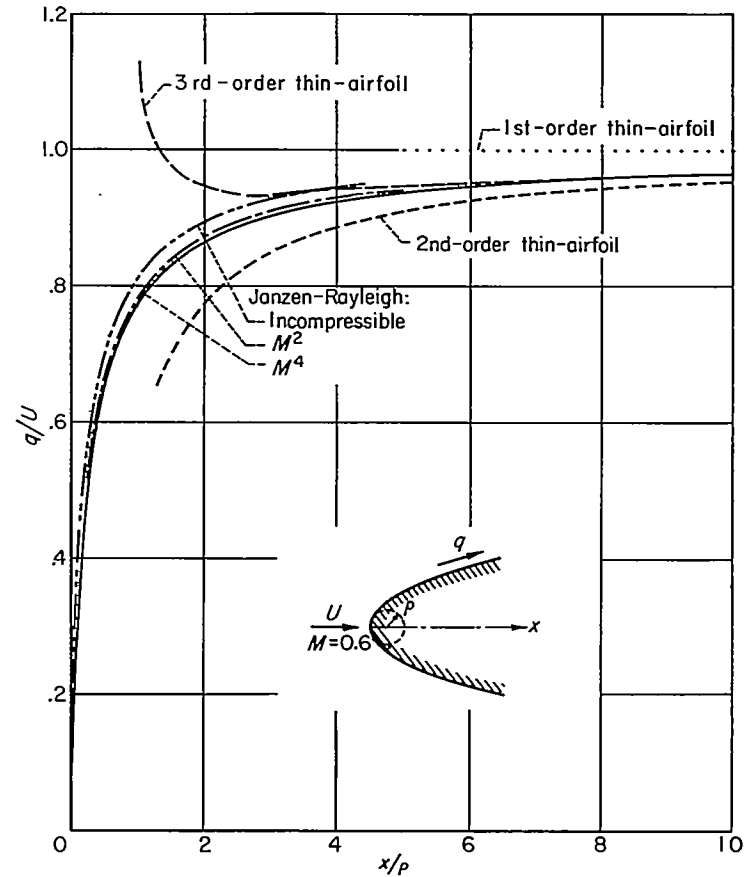
FIGURE 6.—Various approximations for velocity on parabola at $M = 0.6$.

The corresponding table of the function $P[8/(\rho/2), 0, M]$ appearing in equation (34) is:

$$P \left(\frac{8}{\rho/2}, 0, M \right)$$

M \ $8/(\rho/2)$	0.5	1	2	4	10	20	50
0	0.3333	0.5000	0.6667	0.8000	0.9091	0.9524	0.9804
.4	.2924	.4444	.6018	.7339	.8502	.9015	.9402
.5	.2623	.4019	.5500	.6779	.7958	.8507	.8950
.6	.2189	.3391	.4703	.5881	.7025	.7587	.8073
.7	.1607	.2523	.3560	.4531	.5528	.6044	.6517
.8	.0918	.1466	.2111	.2742	.3427	.3797	.4155
.85	.0578	.0932	.1357	.1783	.2256	.2518	.2774
.9	.0284	.0463	.0682	.0906	.1162	.1305	.1437

For other angles of attack, the function Q to order M^2 can be extracted by a limiting process from Kaplan's Janzen-Rayleigh solution (ref. 33) for an inclined ellipse. This gives, with $8/(\rho/2) = X$, $a/\sqrt{\rho/2} = A$

$$Q(X, A, M) = \frac{\sqrt{X} + A}{\sqrt{1+X}} - \frac{M^2}{2(1+X)^{3/2}} \left\{ (1-A^2)\sqrt{X} - A(X+A^2) + \right.$$

$$\frac{1+A^2}{1+X} \left[\left(\sqrt{X} + \frac{1}{2} AX - \frac{1}{2} A \right) \ln \frac{1+X}{4} + \right.$$

$$\left. \left. (1-X+2A\sqrt{X}) \tan^{-1} \sqrt{X} \right] \right\} \qquad (36)$$

The corresponding approximation for the pressure coefficient is

$$\Pi(X,A,M) = \frac{1-2A\sqrt{X}-A^2}{1+X} +$$

$$\frac{M^2}{(1+X)^2}\left\{ \begin{array}{l} \frac{1}{4}(1-2A\sqrt{X}-A^2)^2 + (1-A^2)(X+A\sqrt{X}) - A(X+A^2)(\sqrt{X}+A) + \\[2mm] \frac{(1+A^2)(\sqrt{X}+A)}{1+X}\left[\left(\sqrt{X}+\frac{1}{2}AX-\frac{1}{2}A\right)\ln\frac{1+X}{4} + (1-X+2A\sqrt{X})\tan^{-1}\sqrt{X}\right] \end{array}\right\} \tag{37a}$$

and for the function P, according to equation (34b)

$$P(X,A,M) = \frac{\Pi(X,A,M)}{-2K_1\dfrac{A}{\sqrt{X}}+K_2\left(\dfrac{1}{X}-\dfrac{A^2}{X}\right)} \tag{37b}$$

The error involved in retaining only terms of order M^2 can be estimated from figure 6 in the special case $a=0$. At other angles of attack the error may be greater; in particular, neither the Janzen-Rayleigh expansion nor the thin-airfoil expansion is believed to converge if the local Mach number exceeds unity.

Sharp edges.—The corrections for sharp edges can be found by considering flow in an angle. At a trailing edge with Kutta condition enforced, or a leading edge at ideal angle of attack, the surface and the dividing streamline meet at slightly less than a straight angle, as indicated on the
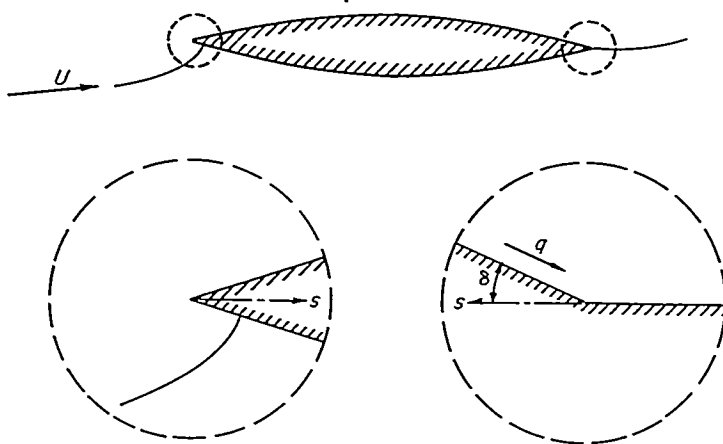

FIGURE 7.—Flow near sharp edges.

right of figure 7. For incompressible flow, the surface speed is found from conformal mapping to be given by

$$\frac{q}{U} = cs^{\frac{\delta}{\pi-\delta}} \tag{38}$$

where δ is the semivertex angle, and s is again measured into the edge. In fixing the constant c, the difficulty that in the angle flow the velocity increases indefinitely upstream can be circumvented by requiring that at any point the velocity must approach that of the free stream as the angle δ tends to zero. Thus it is seen that c is unity except for terms of order δ.

The connection with thin-airfoil theory follows from the fact that for small ϵ

$$s^\epsilon = 1 + \epsilon\ln s + \frac{1}{2}\epsilon^2\log^2 s + \cdots \tag{39}$$

though this relation is not uniformly valid near $s=0$. Hence, the thin-airfoil series for flow in an angle is, to second order,

$$\frac{q_2}{U} = c\left[1 + \frac{\delta}{\pi}\ln s + \frac{\delta^2}{\pi^2}\left(\ln s + \frac{1}{2}\ln^2 s\right)\right] \tag{40}$$

and it is clear how the spurious logarithmic singularities arise.

Comparing these expressions gives a rule that renders the second-order thin-airfoil solution for any sharp-nosed profile uniformly valid:

$$\frac{\bar{q}_2}{U} = s^{\frac{\delta}{\pi-\delta}}\left[\frac{q_2}{U} - \frac{\delta}{\pi}\frac{q_1}{U}\ln s - \frac{\delta^2}{\pi^2}\left(\ln s - \frac{1}{2}\ln^2 s\right)\right] \tag{41}$$

For a leading edge not at the ideal angle of attack, the flow includes a circulatory component, as indicated at the left of figure 7. For incompressible flow, conformal mapping gives the surface speed associated with this component as

$$\frac{q}{U} = \pm as^{-\frac{\pi-2\delta}{2(\pi-\delta)}} \tag{42}$$

and its thin-airfoil expansion is

$$\frac{q_2}{U} = \pm\frac{a}{\sqrt{s}}\left(1 + \frac{\delta}{2\pi}\ln s\right) \tag{43}$$

Comparing these yields a rule for correcting the circulatory component:

$$\frac{\bar{q}_2}{U} = s^{\frac{\delta}{2(\pi-\delta)}}\left(\frac{q_2}{U} - \frac{\delta}{2\pi}\frac{q_1}{U}\ln s\right) \tag{44}$$

The second-order thin-airfoil solution can be treated by splitting off the terms that are singular at least as $s^{-1/2}$ near the leading edge, applying equation (44) to this circulatory component, applying equation (41) to the remainder, and recombining.

These rules could be extended to subsonic speeds, in the case of ideal angle of attack, by calculating the Janzen-Rayleigh solution for flow in an angle. However, at other angles the Janzen-Rayleigh approximation certainly fails, because it would predict infinite speeds that are tolerable only in an incompressible fluid. In any case, the correction is negligible for most practical purposes, because it is significant in only a minute neighborhood of the edge, and, furthermore, sharp edges are usually trailing edges, in which case the details of the flow are masked by viscous effects. For these reasons, no correction for sharp edges is included in the computing scheme given later.

Combined edges.—Airfoils with two stagnation edges are treated by applying the appropriate corrections in turn at

each edge by shifting the origin. Thus, consider an airfoil with round leading and trailing edges of radii ρ_a and ρ_b located at $x=x_a$ and $x=x_b$, respectively, and initial and final camber angles λ_a and λ_b. Assume that the Kutta condition is imposed at the trailing edge. Applying equation (31) twice, identifying s successively with $x-x_a$ and x_b-x, and then simplifying to keep no more than second-order terms gives

$$\frac{\bar{q}_2}{U}=Q\left[\frac{x-x_a\pm\lambda_a\sqrt{2\rho_a(x-x_a)}}{\rho_a/2},\pm\frac{a}{\sqrt{\rho_a/2}},M\right]Q\left[\frac{x_b-x\mp\lambda_b\sqrt{2\rho_b(x_b-x)}}{\rho_b/2},0,M\right]\times$$

$$\left[\frac{q_2}{U}\mp K_1\frac{a}{\sqrt{x-x_a}}\frac{q_1}{U}+\frac{K_2}{4}\left(\frac{\rho_a}{x-x_a}+\frac{\rho_b}{x_b-x}\right)+\left(K_1{}^2-\frac{K_2-1}{2}\right)\frac{a^2}{x-x_a}\right] \quad (45)$$

(The simpler form of this equation for incompressible flow is given as equation (24) of reference 20.) The corresponding rule for pressure coefficient is

$$\bar{C}_{P_2}=P\left[\frac{x-x_a\pm\lambda_a\sqrt{2\rho_a(x-x_a)}}{\rho_a/2},\pm\frac{a}{\sqrt{\rho_a/2}},M\right]\times$$

$$P\left[\frac{x_b-x\mp\lambda_b\sqrt{2\rho_b(x_b-x)}}{\rho_b/2},0,M\right]C_{P_2} \quad (46)$$

Similar rules can be found for combinations of a round and a sharp edge, or two sharp edges. For example, for incompressible flow past two sharp edges of equal angle, both with Kutta condition imposed (as for a symmetrical biconvex airfoil at zero angle of attack) and located at $x=\pm1$, the combined rule has the form of equation (41) with s replaced by $(1-x^2)$.

EXAMPLES: COMPARISON WITH EXPERIMENT AND OTHER THEORIES

INCOMPRESSIBLE FLOW

It has been seen that the solution for subsonic flow depends on that for incompressible flow. It is therefore pertinent to test the second-order theory in the case of incompressible flow, where it can be checked against the exact results of conformal mapping.

Ellipse.—Consider an ellipse of thickness ratio τ with the interval $-1\leq x\leq1$ as chord line. It is described by

$$y=\pm\tau\sqrt{1-x^2}, \qquad -1\leq x\leq1 \quad (47)$$

Suppose that the Kutta condition is satisfied—the rear stagnation point coincides with the end of the major axis. Then the first-order solution for surface speed is found, from equations (3), (4), and (5), together with Appendix B, to be

$$\frac{q_1}{U}=1+\tau\pm\alpha\sqrt{\frac{1-x}{1+x}} \quad (48a)$$

Proceeding with equations (6) to (9) gives the formal second-order result

$$\frac{q_2}{U}=1+\tau\pm\alpha\sqrt{\frac{1-x}{1+x}}-\frac{1}{2}\tau^2\frac{x^2}{1-x^2}\pm\alpha\tau\sqrt{\frac{1-x}{1+x}}-\frac{1}{2}\alpha^2 \quad (48b)$$

This can be checked by expanding the exact result, which is

$$\frac{q}{U}=(1+\tau)\frac{\sqrt{1-x^2}\cos\alpha\pm(1-x)\sin\alpha}{\sqrt{1-x^2+\tau^2x^2}} \quad (49)$$

The formal second-order solution clearly breaks down near the ends of the ellipse. It is converted into a uniformly

valid second approximation by applying equation (21) twice in succession, or using the combined rule of equation (24) of reference 20, which gives

$$\frac{\bar{q}^2}{U}=\sqrt{\frac{1-x^2}{1-x^2+\tau^2}}\left[(1+\tau)\left(1\pm\alpha\sqrt{\frac{1-x}{1+x}}\right)+\frac{1}{2}(\tau^2-\alpha^2)\right] \quad (48c)$$

Exact
○ Modified second-order theory
— — Formal second-order theory
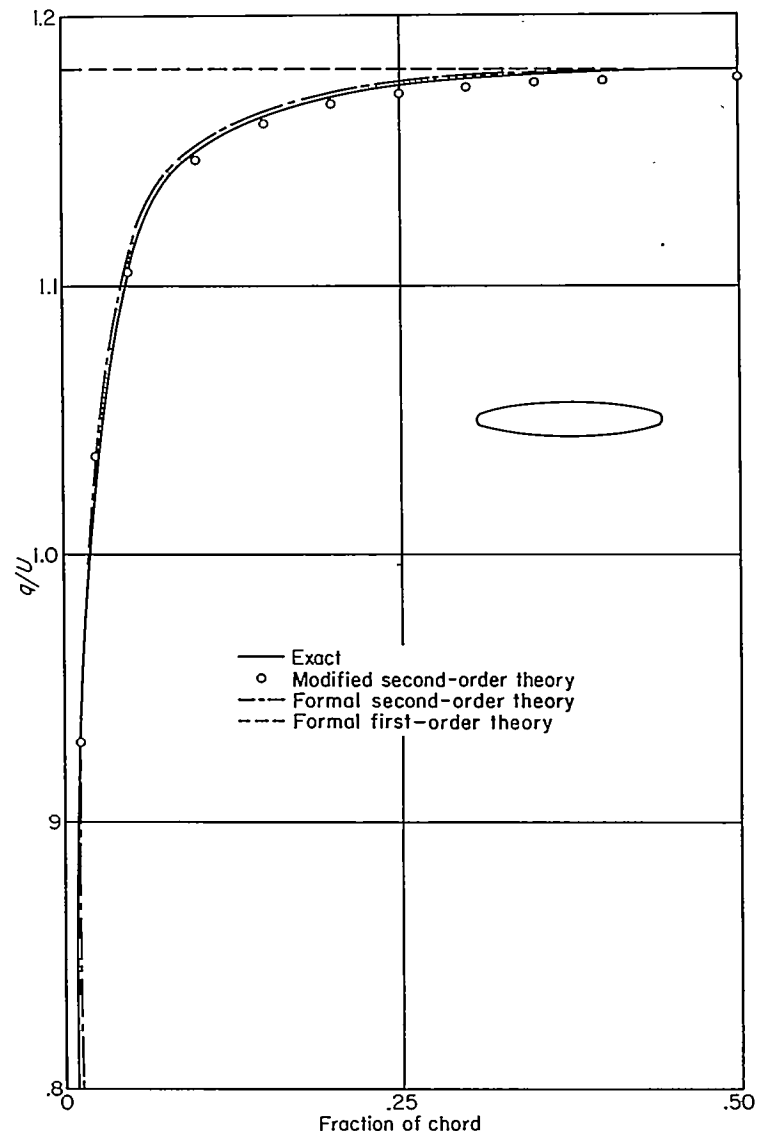-- -- Formal first-order theory

FIGURE 8.—Speed on 18-percent-thick ellipse at zero angle of attack in incompressible flow.

These approximations are compared in figure 8 with the exact solution for an 18-percent-thick ellipse (which has nearly the same nose radius as an NACA 0012 airfoil) at zero angle of attack. The precipitate descent of the formal

second-order solution toward negative infinity is just discernible near the nose and is eliminated by the edge correction.

Symmetrical Joukowski airfoil.—To second as well as first order a symmetrical Joukowski airfoil of thickness ratio τ is described by

$$\left.\begin{array}{l} y=\pm\tau_1(1-x)\sqrt{1-x^2}, \qquad -1\leq x\leq 1 \\[2mm] \tau_1=\dfrac{4}{3\sqrt{3}}\,\tau=0.7698\tau \end{array}\right\} \qquad (50)$$

By the foregoing procedure, the formal second-order solution is found to be

$$\frac{q_2}{U}=1+\tau_1(1-2x)\pm\alpha\sqrt{\frac{1-x}{1+x}}-\frac{1}{2}\tau_1{}^2\frac{1-x}{1+x}(1+2x)^2\mp$$

$$2\tau_1\alpha x\sqrt{\frac{1-x}{1+x}}-\frac{1}{2}\alpha^2 \qquad (51a)$$

where the first three terms give the first-order solution. Correcting this by means of equation (21) with $s=1+x$ and $\rho=4\tau_1{}^2$ (and $\lambda=0$) gives the uniformly valid second approximation

$$\frac{\bar{q}_2}{U}=\sqrt{\frac{1+x}{1+x+2\tau_1{}^2}}\left[1+\tau_1(1-2x)+\frac{1}{2}\tau_1{}^2(1-2x)^2\pm\right.$$

$$\left.\alpha(1-2\tau_1 x)\sqrt{\frac{1-x}{1+x}}-\frac{1}{2}\alpha^2\right] \qquad (51b)$$

In figure 9 these approximations are compared with the exact solution (ref. 34) for a 12-percent-thick section at zero angle of attack. The effect of the edge correction on the second-order result is not discernible to this scale.

Biconvex airfoil.—To second order a symmetrical biconvex airfoil of thickness ratio τ bounded by either circular or parabolic arcs is described by

$$y=\pm\tau(1-x^2), \qquad -1\leq x\leq 1 \qquad (52)$$

The formal second-order solution is found to be

$$\frac{q_2}{U}=1+\frac{2}{\pi}\tau\left(2-x\ln\frac{1+x}{1-x}\right)\pm\alpha\sqrt{\frac{1-x}{1+x}}+\tau^2\left[\frac{3}{\pi^2}\left(2-x\ln\frac{1+x}{1-x}\right)^2-\right.$$

$$\left.\frac{1}{\pi^2}\ln^2\frac{1+x}{1-x}-(1-x^2)\right]\mp\frac{1}{\pi}\alpha\tau\sqrt{\frac{1-x}{1+x}}\left[(1+2x)\ln\frac{1+x}{1-x}-4\right]-\frac{1}{2}\alpha^2$$

$$(53a)$$

In deducing from this a uniformly valid second approximation, the terms independent of α are treated by the rule for combined equal sharp edges that was described just after equation (46), with $\delta=2\tau$. The terms in α are modified according to equation (44) with $s=1+x$. The result is

$$\frac{\bar{q}_2}{U}=(1-x^2)^{\frac{2\tau}{\tau-2\tau}}\left\{1+\frac{2}{\pi}\tau[2-(1+x)\ln(1+x)-(1-x)\ln(1-x)]+\right.$$

$$\left(\frac{2}{\pi}\tau\right)^2\left[3-\frac{\pi^2}{4}(1-x^2)-3(1+x)\ln(1+x)-3(1-x)\ln(1-x)+\right.$$

$$\frac{1}{4}(1+3x)(1+x)\ln^2(1+x)+\frac{1}{4}(1-3x)(1-x)\ln^2(1-x)+$$

$$\left.\frac{3}{2}(1-x^2)\ln(1+x)\ln(1-x)\right]-\frac{1}{2}\alpha^2\right\}\pm\alpha\sqrt{\frac{1-x}{1+x}}(1+x)^{\frac{\tau}{\tau-2\tau}}\left\{1-\right.$$

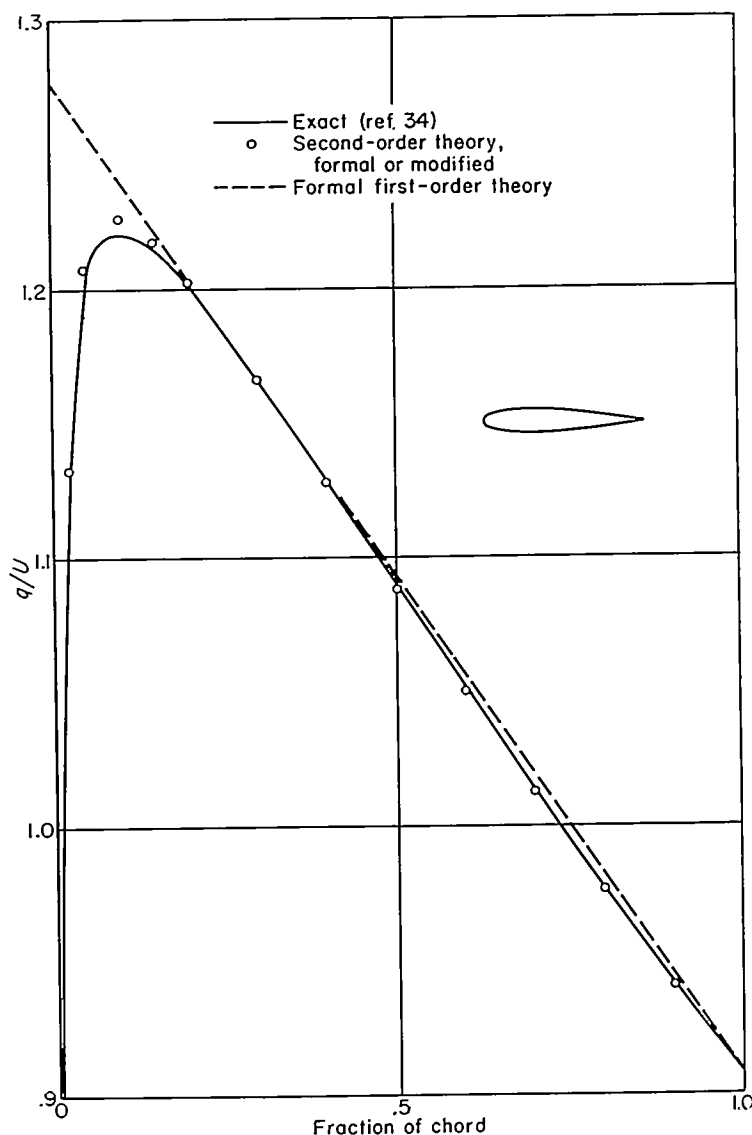$$\left.\frac{\tau}{\pi}[2(1+x)\ln(1+x)-(1+2x)\ln(1-x)-4]\right\} \qquad (53b)$$

FIGURE 9.—Speed on 12-percent-thick symmetrical Joukowski airfoil at zero angle of attack in incompressible flow.
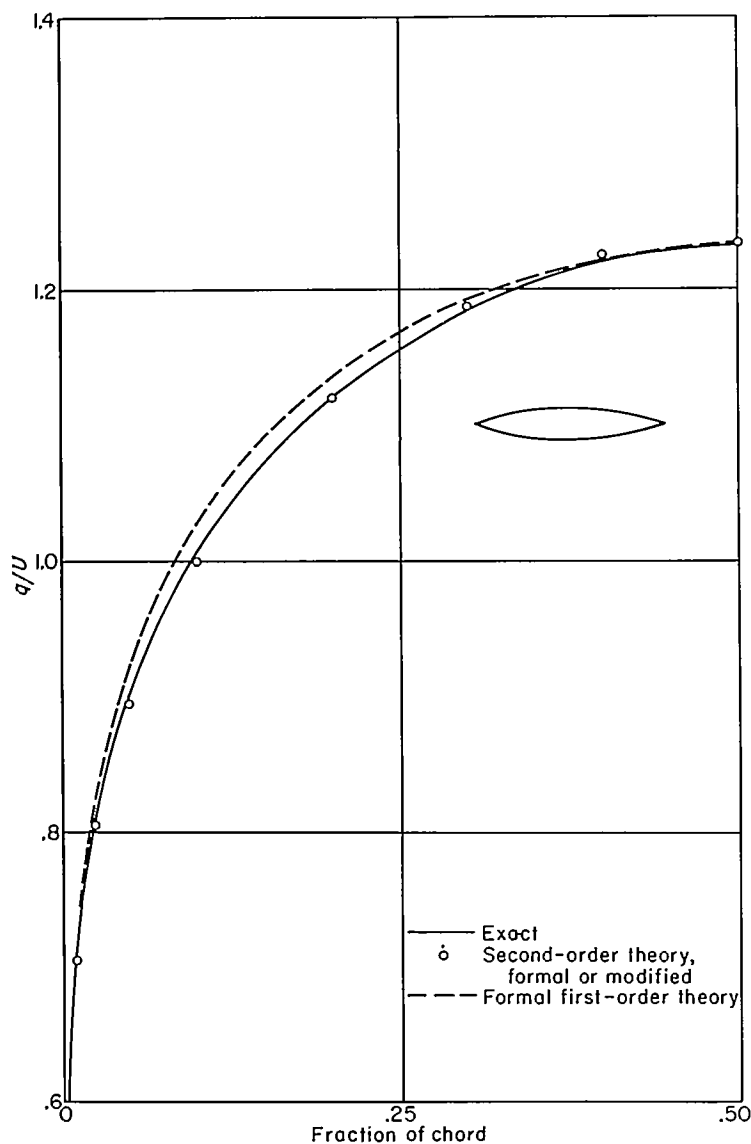
FIGURE 10.—Speed on 18-percent thick biconvex airfoil at zero angle of attack in incompressible flow.

These approximations are compared in figure 10 with the exact solution (ref. 35) for a circular-arc airfoil 18 percent thick at zero angle of attack. Although the vertex angles are large in this example, the edge correction is appreciable in such a small neighborhood of the edge that it would be invisible even on a much larger plot.

NACA 00XX airfoils.—Symmetrical airfoils of the NACA 00XX family (such as the NACA 0012) are naturally defined for the interval $0 \leq x \leq 1$. The airfoil of thickness ratio τ is described by (ref. 36)

$$y = \pm T(x) = \pm \tau(b_1\sqrt{x} + b_2 x + b_4 x^2 + b_6 x^3 + b_8 x^4), \quad 0 \leq x \leq 1 \quad (54)$$

where

$$
\begin{aligned}
b_1 &= 1.48450 \\
b_2 &= -0.63000 \\
b_4 &= -1.75800 \\
b_6 &= 1.42150 \\
b_8 &= -0.50750
\end{aligned}
$$

With the aid of Appendix B the first-order solution is found to be

$$\frac{q_1}{U} = 1 + \frac{\tau}{\pi}\left[\frac{1}{\tau}T'(x)\ln\frac{x}{1-x} + \frac{b_1}{\sqrt{x}}\ln\frac{1+\sqrt{x}}{\sqrt{x}} - 2b_4 - \frac{3}{2}b_6 - \frac{4}{3}b_8 - (3b_6 + 2b_8)x - 4b_8 x^2\right] \pm \alpha\sqrt{\frac{1-x}{x}} \quad (55a)$$

in agreement with the result given by Goldstein (ref. 28). Applying Riegels' rule (eq. (27)) renders this a uniformly valid first approximation except very near the trailing edge.

The second-order terms in thickness, in addition to being very complicated, involve integrals that apparently cannot be evaluated in terms of tabulated functions. Accordingly, the second-order terms have been calculated using the Riegels-Germain numerical method discussed in Appendix C, with $N=16$. The accuracy of this approximation is assured by the fact that cruder approximations modify the numerical results only slightly, as will be seen in a later example.

The formal second-order solution for surface speed therefore has the form

$$\frac{q_2}{U} = 1 + \tau Q_\tau \pm \alpha\sqrt{\frac{1-x}{x}} + \tau^2 Q_{\tau\tau} \pm \tau\alpha Q_{\tau\alpha} - \frac{1}{2}\alpha^2 \quad (55b)$$

where values of Q_τ from equation (55a) and approximate numerical values of $Q_{\tau\tau}$ and $Q_{\tau\alpha}$ are

x	Q_τ	$Q_{\tau\tau}$	$Q_{\tau\alpha}$	x	Q_τ	$Q_{\tau\tau}$	$Q_{\tau\alpha}$
0.025	1.943	−9.00	8.80	0.50	0.900	−0.135	0.32
.05	1.836	−3.35	5.55	.60	.697	−.220	.11
.10	1.714	−1.00	3.25	.70	.485	−.315	−.08
.20	1.510	−.090	1.65	.80	.238	−.410	−.23
.30	1.309	.010	1.00	.90	−.124	−.420	−.33
.40	1.106	−.060	.58	.95	−.440	−.360	−.34

Applying equation (21) with $\rho = 1.10187\ \tau^2$, $\delta = 1.16925\ \tau$ (and $\lambda = 0$) yields a uniformly valid approximation. However, as discussed previously, the curvature of the profile does not vary continuously near its nose, so the result is only a first approximation there, though a second approximation elsewhere.

The various approximations are compared in figure 11 with the result of a "long and elaborate calculation" by conformal mapping for the NACA 0012 airfoil that is given by Goldstein (ref. 37). Again the effect of modifying the second-order solution is indiscernible. Also shown is the "exact" solution tabulated in reference 38. The agreement between the first-order solution with Riegels' rule, the second-order solution, and Goldstein's calculation leaves little doubt that his is the more accurate of the two "exact" solutions.

COMPRESSIBLE FLOW

When extended to subsonic compressible flow, the preceding examples can all be compared with other theories or with
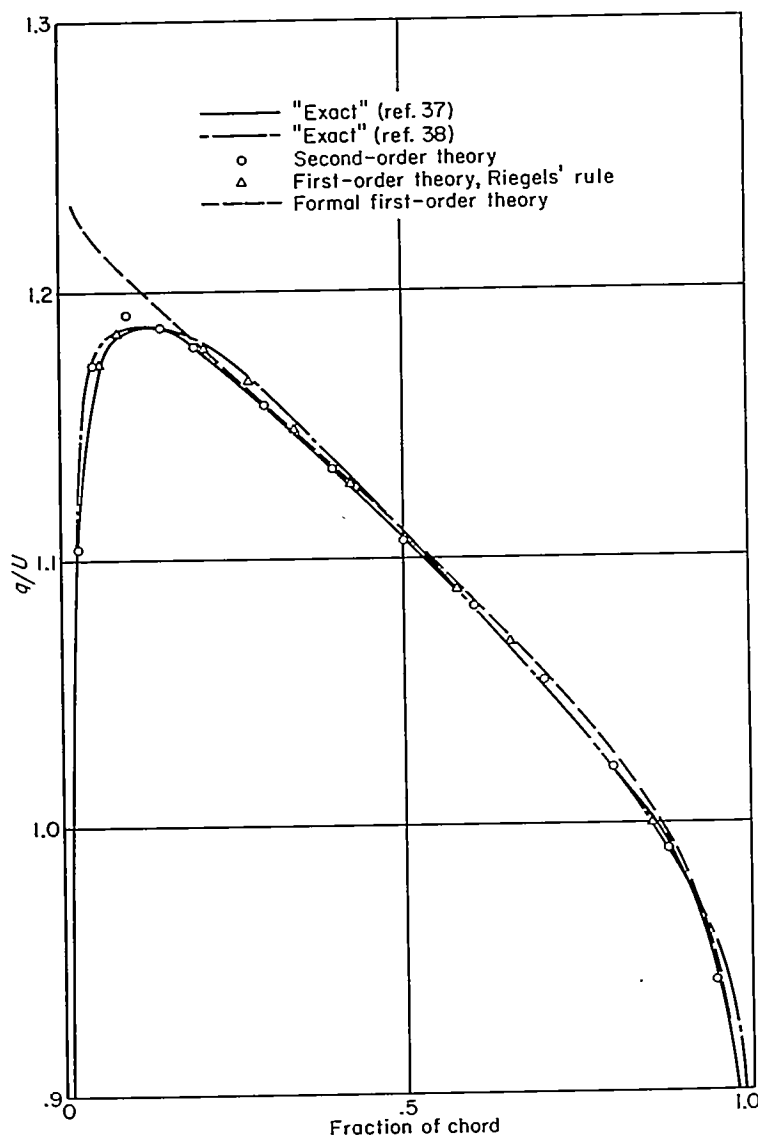
FIGURE 11.—Speed on NACA 0012 airfoil at zero angle of attack in incompressible flow.

experiment. As before, the comparisons will, for simplicity, be made only for zero angle of attack.

Ellipse.—Applying the second-order compressibility rule of equations (13) to the incompressible solution of equation (48b) gives as the formal second-order solution for the speed on an elliptic cylinder

$$\frac{q_2}{U}=1+K_1\left(\tau\pm\alpha\sqrt{\frac{1-x}{1+x}}\right)+\frac{1}{2}\tau^2\left(K_2\frac{1-2x^2}{1-x^2}-1\right)\pm$$

$$\tau\alpha(2K_2-1)\sqrt{\frac{1-x}{1+x}}-\alpha^2\frac{1+(2K_2-1)x}{2(1+x)} \qquad (56)$$

For zero angle of attack the maximum speed, occurring at midchord, is given by

$$\left(\frac{q_2}{U}\right)_{max}=1+K_1\tau+\frac{1}{2}(K_2-1)\tau^2 \qquad (57)$$

in agreement with the result of Hantzsche and Wendt (ref. 7) The corresponding third-order result has been given by Hantzsche (ref. 8); his expression can be simplified to

$$\left(\frac{q_3}{U}\right)_{max}=1+K_1\tau+\frac{1}{2}(K_2-1)\tau^2+\frac{M^2}{\beta^3}\left\{\frac{\pi}{4}\left[1+\frac{n}{4}\left(1+\frac{n}{2}\right)(8-M^2)\right]-\right.$$
$$\left.\left(\frac{1}{2}+\frac{3}{4}n+\frac{1}{3}n^2\right)\right\}\tau^3-\frac{M^2}{2\beta^2}\left[1+\right.$$
$$\left.\frac{n}{4}\left(1+\frac{n}{2}\right)(8-M^2)\right]\tau^4\ln\frac{1}{\tau}+0(\tau^4) \qquad (58a)$$

where

$$n=\frac{\gamma+1}{2}\frac{M^2}{\beta^2} \qquad (58b)$$

The terms in $\tau^4\ln\tau$ are found correct together with those in τ^3 in the second iteration; it is a matter of taste whether they are regarded as being of third or fourth order. The solution to τ^3 has subsequently been given by Hasimoto (ref. 39), and although typographical errors unfortunately appear in his equations, his numerical results agree with those calculated from equation (58a).

Values of the maximum speed ratio calculated from these and other approximations for a 10-percent-thick ellipse at zero angle of attack (whose critical Mach number is about 0.80) are:

	$M=0.70$	$M=0.75$	$M=0.80$
First-order theory (or Prandtl-Glauert rule applied to exact incompressible value of 1.1)	1.140	1.151	1.167
Kármán-Tsien rule	1.149	1.163	1.184
Second-order theory	1.148	1.163	1.185
Third-order theory;			
including τ^3	1.150	1.167	1.196
including $\tau^4\ln\tau$	1.149	1.166	1.194

(Here the Kármán-Tsien rule has been applied to the pressure coefficient for incompressible flow, and the speed ratio then calculated from Bernoulli's equation.) It might have been anticipated that the second-order theory is more accurate than any of the compressibility correction formulas such as the Kármán-Tsien rule, because it allows for a dependence on the particular airfoil shape and on the value of γ. However, in this example the results of second-order theory and the Kármán-Tsien rule are practically identical.

In the same way the second-order solutions are readily calculated for the Joukowski and the biconvex airfoils, and are found to agree with the results that Hantzsche and Wendt obtained by laborious analysis.

NACA 0012 airfoil.—The formal first- and second-order solutions for NACA 00XX airfoils in subsonic flow are easily obtained from equations (13) and (55). The second-order solution can then be rendered uniformly valid near the nose using equation (31), although again the modification is significant in only a very small region of the nose.

For the NACA 0012 airfoil at zero angle of attack, Emmons has calculated the flow field at Mach numbers of 0, 0.70, and 0.75 using the numerical relaxation method (ref. 40). The last of these Mach numbers is supercritical, so that the flow contains shock waves, and is beyond the scope of the present theory. The pressure distribution calculated
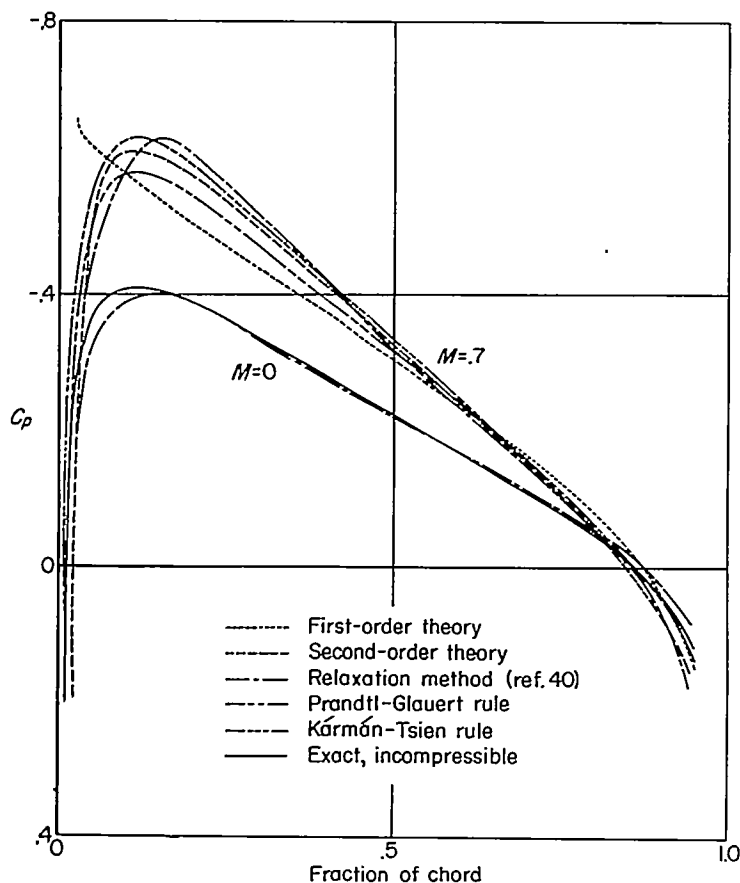
FIGURE 12.—Pressure coefficient on NACA 0012 airfoil at zero angle of attack in subsonic flow.

FIGURE 13.—Comparison of theoretical and experimental pressure distributions on NACA 0015 airfoil at $M=0.70$, zero angle of attack.

by the relaxation method for $M=0.70$ is compared in figure 12 with the results of first- and second-order theory and various other approximations. The relaxation solution for incompressible flow is also shown in comparison with Goldstein's "exact" solution, and is seen to be inaccurate near the nose. The solution for $M=0.70$ probably contains similar inaccuracies; however, just as for the ellipse the pressure coefficients calculated by second-order theory may be slightly less negative than the true values near the minimum.

Experiments on NACA 0015 airfoil.—Experimental pressure distributions in two-dimensional flow over the NACA 0015 airfoil at high subsonic speeds are reported in reference 41. For zero angle of attack, the critical Mach number is approximately 0.70. The measurements at this Mach number are compared in figure 13 with the results of first- and second-order theory and of the two common compressibility correction formulas applied to the incompressible flow values tabulated in reference 38. Unfortunately, the model was imperfectly constructed, and the ordinates were inaccurate near the nose and midchord. Otherwise, the measured pressures are in satisfactory accord with either second-order theory or the results of the Kármán-Tsien rule.

Tomotika and Tamada's airfoil.—Using the hodograph method, Tomotika and Tamada have calculated the flow past a certain family of symmetric airfoils (ref. 42). As usual in hodograph solutions, the airfoil shape varies somewhat with free-stream Mach number. The critical Mach

number is 0.717, and the corresponding shape is shown in figure 14 together with the surface speeds predicted by various theories.

For mathematical simplicity, Tomotika and Tamada have adopted a hypothetical gas, which is fitted at Mach numbers zero and unity to a polytropic gas having $\gamma=7/5$. At any intermediate Mach number, however, the hypothetical gas corresponds to a polytropic gas whose γ is greater than $7/5$, reaching a maximum value of 1.91 at $M=0.78$. To second order, any such hypothetical gas is equivalent to a polytropic gas having the value of γ corresponding to the free-stream flow, given by

$$\gamma=1+\left(\frac{\rho}{c^2}\frac{dc^2}{d\rho}\right)_{\text{free-stream}}$$

where ρ is the density and c the speed of sound in the hypothetical gas. For Tomotika and Tamada's gas with $M=0.717$, that value is 1.82. Actually, the second-order solution depends so slightly upon the value of γ that the change from $\gamma=7/5$ to $\gamma=1.82$ increases the maximum value of q/U by only two parts in a thousand. However, the nonpolytropic
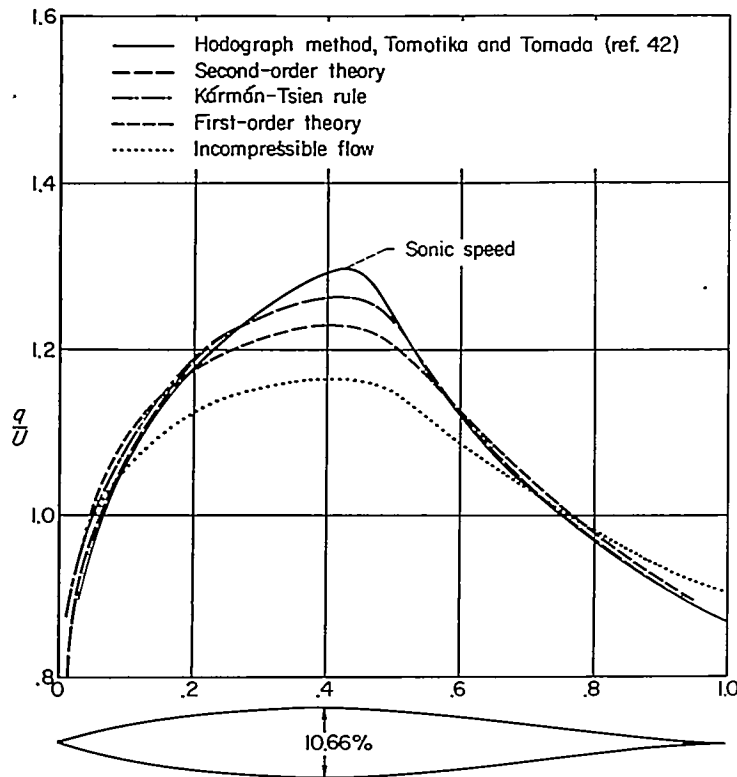
FIGURE 14.—Speed on Tomotika-Tamada airfoil at $M=0.717$.

nature of the hypothetical gas must be considered in converting Tomotika and Tamada's values of surface speed (which are referred to the critical speed) to the form q/U. At the free-stream Mach number of 0.717, the ratio of freestream to critical speeds is 0.769 for the hypothetical gas, compared with 0.748 for a polytropic gas having $\gamma=7/5$ (and 0.774 for a polytropic gas having $\gamma=1.82$).[4] Thus, as Tomotika and Tamada emphasize, their results should be regarded as exact for the hypothetical gas; and the present method should be regarded as giving the true second approximation for the same gas (which to second order is equivalent to a polytropic gas with $\gamma=1.82$).

The agreement between the hodograph method and second-order theory is satisfactory. Third- and higher-order terms are seen to increase the surface speed near its maximum and reduce it slightly elsewhere, which is the effect of third-order terms calculated by Asaka for a biconvex airfoil (ref. 43).

As shown in figure 14, the results of second-order theory and the Kármán-Tsien rule nearly coincide except over the forward portion, where the second-order theory is apparently more accurate. The second-order solution calculated with the present computing scheme is in close agreement with an unpublished second-order solution carried out by Naruse.

PRACTICAL NUMERICAL COMPUTATION

The following computing procedure yields the second-order subsonic solution for the surface speed or pressure on any air-

foil at any angle of attack. It requires a knowledge only of the airfoil ordinates at 7 (or 15) points along the chord. It is based on the foregoing theory together with the numerical method of Riegels and Germain that is discussed in Appendix C. It includes the correction for a round leading edge, but not for sharp edges.

COMPUTING PROCEDURE WITH $N=8$ (OR 16)

(1) Tabulate the ordinates Y_u and Y_l of the upper and lower surfaces at the 7 (15) pivotal points x_n listed in table I. (The x axis must pass through the leading and trailing edges with the leading edge at $x=0$ and trailing edge at $x=1$.)

(2) Calculate the corresponding values of

$$T=\tfrac{1}{2}(Y_u-Y_l), \qquad C=\tfrac{1}{2}(Y_u+Y_l) \qquad (59)$$

(3) Using the influence coefficients of tables II, III, and IV, calculate

$$\left. \begin{array}{ll} \dfrac{u_{1t}}{U}=\sum_{s=1}^{7(15)} c_{ns}T_s & \dfrac{u_{1c}^{*}}{U}=\sum_{s=1}^{7(15)} d_{ns}C_s \\[2mm] T'=\sum_{s=1}^{7(15)} e_{ns}T_s & C'=\sum_{s=1}^{7(15)} f_{ns}C_s \\[2mm] T''=\sum_{s=1}^{7(15)} g_{ns}T_s & C''=\sum_{s=1}^{7(15)} h_{ns}C_s \end{array} \right\} \qquad (60)$$

(4) Using table I (with α in radians), calculate

$$\frac{u_{1c}}{U}=\frac{u_{1c}^{*}}{U}+\alpha\sqrt{\frac{1-x}{x}} \qquad (61)$$

(5) Calculate

$$T_2=\frac{u_{1t}}{U}T+\frac{u_{1c}}{U}C, \qquad C_2=\frac{u_{1t}}{U}C+\frac{u_{1c}}{U}T \qquad (62)$$

(6) Using the influence coefficients of table II, calculate

$$\frac{u_{2t}}{U}\sum_{s=1}^{7(15)} c_{ns}T_{2s}-\frac{1}{2}\alpha^2, \qquad \frac{u_{2c}}{U}=\sum_{s=1}^{7(15)} d_{ns}C_{2s} \qquad (63)$$

(7) Using the compressibility factors of table V, calculate

$$\frac{q_2}{U}=1+K_1\frac{u_{1t}}{U}+K_2\left(\frac{u_{2t}}{U}+CC''+TT''+\frac{1}{2}C'^2+\frac{1}{2}T'^2\right)+ \cdot$$

$$\frac{K_2-1}{2}\left[\left(\frac{u_{1t}}{U}\right)^2+\left(\frac{u_{1c}}{U}\right)^2\right]\pm\left[K_1\frac{u_{1c}}{U}+K_2\left(\frac{u_{2c}}{U}+CT''+\right.\right.$$

$$\left.\left.C''T+C'T'\right)+(K_2-1)\frac{u_{1t}}{U}\frac{u_{1c}}{U}\right] \qquad (64a)$$

or

$$C_{p2}=-2K_1\left(\frac{u_{1t}}{U}\pm\frac{u_{1c}}{U}\right)-K_2\left[2\frac{u_{2t}}{U}\pm2\frac{u_{2c}}{U}+\right.$$

$$\left.2(C\pm T)(C''\pm T'')+(C'\pm T')^2+\left(\frac{u_{1t}}{U}\pm\frac{u_{1c}}{U}\right)^2\right] \qquad (64b)$$

The $\pm$ signs refer to the upper and lower surfaces of the airfoil.

---

[4] The author is indebted to Mr. H. Naruse of Tokyo Metropolitan University for having pointed out these ideas, some of which stem in turn from his colleagues, I. Imai and H. Takami.

Correction for round leading edge.—If the airfoil has a round leading edge, continue as follows:

(8) Using the influence coefficients of table I, calculate

$$\sqrt{\frac{\rho}{2}}=\sum_{n=1}^{7(15)} r_n T_n, \qquad \lambda=\sum_{n=1}^{7(15)} f_n C_n, \tag{65}$$

$$a_1{}^*=\sum_{n=1}^{7(15)} d_n C_n, \qquad a_2{}^*=\sum_{n=1}^{7(15)} d_n C_{2n} \tag{66}$$

(9) Calculate

$$a=\sqrt{2}(\alpha+a_1{}^*+a_2{}^*)+\frac{1}{2}\lambda\sqrt{\frac{\rho}{2}} \tag{67}$$

$$A=\frac{a}{\sqrt{\rho/2}} \tag{68}$$

(10) At each pivotal point on the upper and lower surfaces calculate

$$X_n=\frac{x_n\pm\lambda\sqrt{2\rho x_n}}{\rho/2} \tag{69}$$

and then calculate

$$Q(X_n,\pm A, M) \qquad \text{or} \qquad P(X_n,\pm A, M) \tag{70}$$

from equation (36) or (37)

(11) Using the compressibility factors of table V, calculate at each point

$$\frac{q_2}{U}=Q\left[\frac{q_2}{U}\mp K_1\frac{a}{\sqrt{x}}\left(1+\frac{u_{1t}}{U}\pm\frac{u_{1c}}{U}\right)+\frac{K_2}{4}\frac{\rho}{x}+\left(K_1{}^2-\frac{K_2-1}{2}\right)\frac{a^2}{x}\right] \tag{71a}$$

or

$$\overline{C}_{p_2}=PC_{p_2} \tag{71b}$$

REMARKS

1. The summations of steps (3), (6), and (8) are conveniently carried out by tabulating C and T in columns that can be matched with successive columns of tables II and III while cumulative multiplication is carried out on a desk calculating machine.

2. If the airfoil slope and second derivative can be found more directly, step (3) can be simplified by omitting the calculation of T', C', T'', and C''.

3. If the leading-edge radius ρ and initial camber angle λ are known, omit their calculation from step (8).

4. Seven pivotal points yield sufficient accuracy for most purposes. If conditions near the nose of a thin airfoil are of interest it may be necessary to repeat the computation using 15 pivotal points.

5. The above scheme is designed for calculating a single case. If the same airfoil is to be calculated at more than two angles of attack, it is economical to subdivide the computing scheme to separate terms in α and α^2. Similarly, the scheme should be subdivided if more than two thickness or camber ratios are to be calculated for the same family of airfoils.

6. For NACA airfoils T is the basic thickness and C the camber line. To second order it is immaterial that the thickness is added normal to the camber line rather than to the chord line.

7. In step (10), if $A=0$ the values of Q or P can be taken from the tables following equation (35).

EXAMPLE

The following table gives the complete computing form for calculating the first- and second-order increments in surface speed for an NACA 00XX airfoil (of unit thickness ratio) at zero angle of attack and zero Mach number:

n	x	T	$\dfrac{u_{1t}}{U}=\dfrac{\Delta q_1}{U}$	T'	T''	T_1	$\dfrac{u_{2t}}{U}$	$\dfrac{\Delta q_1}{U}$
1	0.03806	0.26316	1.8936	3.0914	−54.721	0.48832	4.8040	−4.8180
2	.14645	.44236	1.6158	.8652	−8.928	.71478	3.1691	−.4062
3	.30866	.49990	1.2906	−.0235	−3.638	.64517	1.8200	.0028
4	.50000	.44051	.9053	−.5445	−1.989	.39379	.5719	−.1340
5	.69134	.30843	.4909	−.8063	−1.048	.15142	−.3081	−.3063
6	.85355	.16199	.0824	−1.0163	−1.574	.01335	−.6913	−.4293
7	.96194	.04499	−.5951	−1.0879	1.643	−.02677	−.9888	−.3230

The accuracy of this solution with only 7 pivotal points is indicated by comparison with the following values, which were obtained analytically for $\Delta q_1/U$ and with 15 pivotal points for $\Delta q_2/U$:

x	$\dfrac{u_{1t}}{U}=\dfrac{\Delta q_1}{U}$	$\dfrac{\Delta q_2}{U}$
0.14645	1.6166	−0.4009
.50000	.9003	−.1348
.85355	.0725	−.4239

It is seen that the solution using 7 pivotal points yields ample accuracy.

AMES AERONAUTICAL LABORATORY
NATIONAL ADVISORY COMMITTEE FOR AERONAUTICS
MOFFETT FIELD, CALIF., *March 12, 1956*

APPENDIX A

PRINCIPAL SYMBOLS

A	$a/\sqrt{\rho/2}$
a	factor proportional to angle of attack measured from ideal angle
b_n	coefficient of $x^{n/2}$ in series for airfoil ordinate
$C(x)$	camber of airfoil
$C_2(x)$	camber of fictitious airfoil in second-order solution
C_p	surface-pressure coefficient
C_{p_1}	first-order surface-pressure coefficient
ΔC_{p_2}	second-order increment in surface-pressure coefficient
$c_{ns}, d_{ns}, e_{ns},$ f_{ns}, g_{ns}, h_{ns}	influence coefficients for calculating velocity, slope, and second derivative of airfoil ordinate
d_n	influence coefficient for calculating a
$f(z)$	analytic function of complex variable
f_n	f_{on}, influence coefficient for calculating initial camber angle
I	imaginary part of $f(z)$ on unit circle
K_1	first-order compressibility factor, $\dfrac{1}{\beta}$
K_2	second-order compressibility factor, $\dfrac{(\gamma+1)M^4+4\beta^2}{4\beta^4}$
k_r	coefficient in trigonometric polynomial approximation to C
M	free-stream Mach number
N	number of subdivisions of chord line in numerical integration
P	ratio of pressure coefficient on parabola in subsonic flow to second-order thin-airfoil value
Q	surface speed ratio on parabola in subsonic flow
$Q_r, Q_{rr}, Q_{r\alpha}$	(See eq. (55b).)
q	flow speed on surface of airfoil
$\Delta q_1, \Delta q_2$	first- and second-order increments in q
R	real part of $f(z)$ on unit circle
r	influence coefficient for calculating edge radius
s	abscissae measured from edge positive into airfoil
s	distance from round edge measured along initial tangent to camber line
$T(x)$	thickness of airfoil
$T_2(x)$	thickness of fictitious airfoil in second-order solution

t_r	coefficient in trigonometric polynomial approximation to T
U	free-stream speed
u	velocity perturbation parallel to chord line
v	velocity perturbation normal to chord line
x	abscissa
X	$s/(\rho/2)$
$Y(x)$	ordinate of airfoil
Y_u, Y_l	ordinates of upper and lower surfaces of airfoil, respectively
y	ordinate
z	complex variable
α	angle of attack
β	$\sqrt{1-M^2}$
β_p	coefficient in numerical calculation of u
γ	adiabatic exponent of gas
γ_p	coefficient in numerical calculation of Y'
δ	semivertex angle of sharp edge
θ	polar angle
η	angle of airfoil surface to chord line
λ	terminal angle of camber line to chord line
μ_p	coefficient in numerical calculation of Y''
Π	pressure coefficient on parabola in subsonic flow
ρ	radius of round edge
τ	airfoil thickness ratio
τ_1	$\dfrac{4}{3\sqrt{3}}\tau$ for Joukowski airfoil
φ	perturbation velocity potential
ψ	perturbation stream function
$(\ )_a$	value at leading edge
$(\ )_b$	value at trailing edge
$(\ )_c$	component associated with camber and angle of attack
$(\ )_M$	value at Mach number M
$(\ )_m$	value at mth pivotal point counted from trailing edge
$(\ )_n$	value at nth pivotal point counted from leading edge
$(\ )_p$	index of summation, counted from trailing edge
$(\ )_s$	index of summation, counted from leading edge
$(\ )_t$	component associated with thickness
$(\ )_0$	value at zero Mach number
$(\ )_1$	first-order approximation
$(\ )_2$	second-order approximation
$(\ )'$	derivative
$(\bar{\ })$	uniformly valid approximation

APPENDIX B

AIRFOIL INTEGRALS

The following are the Cauchy principal values for $x^2 \leq 1$:

1. $\displaystyle\oint_{-1}^{1} \frac{1}{x-\xi}\, d\xi = \ln\frac{1+x}{1-x}$

2. $\displaystyle\oint_{-1}^{1} \frac{\xi}{x-\xi}\, d\xi = x\ln\frac{1+x}{1-x} - 2$

3. $\displaystyle\oint_{-1}^{1} \frac{\xi^2}{x-\xi}\, d\xi = x\left(x\ln\frac{1+x}{1-x} - 2\right)$

4. $\displaystyle\oint_{-1}^{1} \frac{\xi^3}{x-\xi}\, d\xi = x^2\left(x\ln\frac{1+x}{1-x} - 2\right) - \frac{2}{3}$

5. $\displaystyle\oint_{-1}^{1} \frac{\xi^n}{x-\xi}\, d\xi = x\oint_{-1}^{1} \frac{\xi^{n-1}}{x-\xi}\, d\xi - \frac{1-(-1)^n}{n}$

6. $\displaystyle\oint_{-1}^{1} \frac{1}{\sqrt{1-\xi^2}\,(x-\xi)}\, d\xi = 0$

7. $\displaystyle\oint_{-1}^{1} \frac{\xi}{\sqrt{1-\xi^2}\,(x-\xi)}\, d\xi = -\pi$

8. $\displaystyle\oint_{-1}^{1} \frac{\xi^2}{\sqrt{1-\xi^2}\,(x-\xi)}\, d\xi = -\pi x$

9. $\displaystyle\oint_{-1}^{1} \frac{\xi^3}{\sqrt{1-\xi^2}\,(x-\xi)}\, d\xi = -\pi\left(x^2+\frac{1}{2}\right)$

10. $\displaystyle\oint_{-1}^{1} \frac{\xi^4}{\sqrt{1-\xi^2}\,(x-\xi)}\, d\xi = -\pi x\left(x^2+\frac{1}{2}\right)$

11. $\displaystyle\oint_{-1}^{1} \frac{\xi^5}{\sqrt{1-\xi^2}(x-\xi)}\, d\xi = -\pi\left(x^4+\frac{1}{2}x^2+\frac{3}{8}\right)$

12. $\displaystyle\oint_{-1}^{1} \frac{\xi^6}{\sqrt{1-\xi^2}(x-\xi)}\, d\xi = -\pi x\left(x^4+\frac{1}{2}x^2+\frac{3}{8}\right)$

13. $\displaystyle\oint_{-1}^{1} \frac{\xi^n}{\sqrt{1-\xi^2}(x-\xi)}\, d\xi = x\oint_{-1}^{1} \frac{\xi^{n-1}}{\sqrt{1-\xi^2}(x-\xi)}\, d\xi -$

$$\frac{\pi}{2}\left[1-(-1)^n\right]\frac{1(3)\ldots(n-2)}{2(4)\ldots(n-1)}$$

14. $\displaystyle\oint_{-1}^{1} \frac{\sqrt{1-\xi^2}}{x-\xi}\, d\xi = \pi x$

15. $\displaystyle\oint_{-1}^{1} \frac{\xi\sqrt{1-\xi^2}}{x-\xi}\, d\xi = \pi\left(x^2-\frac{1}{2}\right)$

16. $\displaystyle\oint_{-1}^{1} \frac{\xi^2\sqrt{1-\xi^2}}{x-\xi}\, d\xi = \pi x\left(x^2-\frac{1}{2}\right)$

17. $\displaystyle\oint_{-1}^{1} \frac{\xi^3\sqrt{1-\xi^2}}{x-\xi}\, d\xi = \pi\left(x^4-\frac{1}{2}x^2-\frac{1}{8}\right)$

18. $\displaystyle\oint_{-1}^{1} \frac{\sqrt{1+\xi}}{\sqrt{1-\xi}(x-\xi)}\, d\xi = -\pi$

19. $\displaystyle\oint_{-1}^{1} \frac{\ln\frac{1+\xi}{1-\xi}}{x-\xi}\, d\xi = \frac{1}{2}\left(\ln^2\frac{1+x}{1-x} - \pi^2\right)$

20. $\displaystyle\oint_{-1}^{1} \frac{\xi\ln\frac{1+\xi}{1-\xi}}{x-\xi}\, d\xi = \frac{1}{2}x\left(\ln^2\frac{1+x}{1-x} - \pi^2\right)$

21. $\displaystyle\oint_{-1}^{1} \frac{\xi^2\ln\frac{1+\xi}{1-\xi}}{x-\xi}\, d\xi = \frac{1}{2}x^2\left(\ln^2\frac{1+x}{1-x} - \pi^2\right) - 2$

22. $\displaystyle\oint_{-1}^{1} \frac{\xi^3\ln\frac{1+\xi}{1-\xi}}{x-\xi}\, d\xi = \frac{1}{2}x^3\left(\ln^2\frac{1+x}{1-x} - \pi^2\right) - 2x$

23. $\displaystyle\oint_{-1}^{1} \frac{\xi^4\ln\frac{1+\xi}{1-\xi}}{x-\xi}\, d\xi = \frac{1}{2}x^4\left(\ln^2\frac{1+x}{1-x} - \pi^2\right) - 2x^2 - \frac{4}{3}$

24. $\displaystyle\oint_{-1}^{1} \frac{\xi^n\ln\frac{1+\xi}{1-\xi}}{x-\xi}\, d\xi = x\oint_{-1}^{1} \frac{\xi^{n-1}\ln\frac{1+\xi}{1-\xi}}{x-\xi}\, d\xi -$

$$\frac{2}{n}\left[1-(-1)^{n-1}\right]\sum_{\nu=0}^{\frac{n}{2}-1}\frac{1}{n-1-2\nu}$$

25. $\displaystyle\oint_{-1}^{1} \frac{1}{\sqrt{1+\xi}(x-\xi)}\, d\xi = \frac{1}{\sqrt{1+x}}\ln\frac{\sqrt{2}+\sqrt{1+x}}{\sqrt{2}-\sqrt{1+x}}$

26. $\displaystyle\oint_{-1}^{1} \frac{\sqrt{1+\xi}}{x-\xi}\, d\xi = \sqrt{1+x}\ln\frac{\sqrt{2}+\sqrt{1+x}}{\sqrt{2}-\sqrt{1+x}} - 2\sqrt{2}$

27. $\displaystyle\oint_{-1}^{1} \frac{\ln\frac{1+\xi}{1-\xi}}{\sqrt{1-\xi^2}(x-\xi)}\, d\xi = -\frac{\pi^2}{\sqrt{1-x^2}}$

28. $\displaystyle\oint_{-1}^{1} \frac{\xi\ln\frac{1+\xi}{1-\xi}}{\sqrt{1-\xi^2}(x-\xi)}\, d\xi = -\pi^2\frac{x}{\sqrt{1-x^2}}$

29. $\displaystyle\oint_{-1}^{1} \frac{\xi^2\ln\frac{1+\xi}{1-\xi}}{\sqrt{1-\xi^2}(x-\xi)}\, d\xi = -\pi\left(2+\pi\frac{x^2}{\sqrt{1-x^2}}\right)$

30. $\displaystyle\oint_{-1}^{1} \frac{\xi^3\ln\frac{1+\xi}{1-\xi}}{\sqrt{1-x^2}(x-\xi)}\, d\xi = -\pi x\left(2+\pi\frac{x^2}{\sqrt{1-x^2}}\right)$

31. $\displaystyle\oint_{-1}^{1} \frac{\xi^4\ln\frac{1+\xi}{1-\xi}}{\sqrt{1-\xi^2}(x-\xi)}\, d\xi = -\pi\left(\frac{5}{3}+2x^2+\pi\frac{x^4}{\sqrt{1-x^2}}\right)$

32. $\displaystyle\oint_{-1}^{1} \frac{\xi^n\ln\frac{1+\xi}{1-\xi}}{\sqrt{1-\xi^2}(x-\xi)}\, d\xi = x\int_{-1}^{1} \frac{\xi^{n-1}\ln\frac{1+\xi}{1-\xi}}{\sqrt{1-\xi^2}(x-\xi)}\, d\xi -$

$$\pi\left[1-(-1)^{n-1}\right]\left(\frac{n}{2}-1\right)!\sum_{0}^{\frac{n}{2}-1}\frac{(-1)^\nu(1)(3)\ldots(\nu)}{2^\nu(2\nu+1)(\nu!)^2\left(\frac{n}{2}-1-\nu\right)!}$$

APPENDIX C

THE RIEGELS-GERMAIN METHOD

The numerical procedure introduced by Riegels (ref. 2) and Germain (ref. 21) can be adapted to give approximately the thin-airfoil velocities on any profile in terms of its ordinates at certain fixed points. Thwaites has applied Germain's procedure to thin-airfoil theory (ref. 23), and Weber has systematized the calculation of the slope and surface velocity (refs. 24 and 25). Here we must also find the second derivative. In applying the edge correction at a round nose we also require the edge radius. It is convenient to derive all these results from Watson's analysis (ref. 22).

Let $f(z)$ be regular within the unit circle, and on the unit circle have the form

$$f(e^{i\theta})=R(\theta)+iI(\theta) \tag{C1}$$

(Our R and I are Watson's ψ and ϵ.) Then following Germain, Watson approximates to R by the trigonometric polynomial

$$R(\theta)\approx k_0+\sum_{r=1}^{N-1}(k_r\cos r\theta+t_r\sin r\theta)+k_N\cos N\theta \tag{C2}$$

which can be made to coincide with R at the $2N$ equally spaced pivotal points $\theta=\theta_m=m\pi/N$. Thus he derives approximate formulas for I (aside from a constant), R', I', $\int R$, and $\int I$ in terms of the values of R at the pivotal points times fixed influence coefficients.

In thin-airfoil theory the complex perturbation potential $\varphi+i\psi$ is regular outside the unit circle in the absence of circulation. Inversion shows that this involves a change in sign of either the real or imaginary part, since $f(e^{-i\theta})=R-iI$. Hence $(\varphi,-\psi)$ or (ψ,φ) may be identified with (R,I).

In thin-airfoil theory the tangency condition on the perturbation stream function ψ is $\psi=-Y$, where Y is the airfoil ordinate. Therefore, in order to obtain a solution in terms of the airfoil ordinates we identify $(Y,-\varphi)$ with (R,I). It is assumed throughout that the x axis passes through the leading and trailing edges.

STREAMWISE VELOCITY INCREMENT FOR $\alpha=0$

Let x run from 0 at the leading edge of the airfoil to 1 at the trailing edge, and

$$x=\frac{1}{2}(1+\cos\theta) \tag{C3}$$

Then the streamwise perturbation velocity on the airfoil is given by

$$\frac{u}{U}=\frac{\partial\varphi}{\partial x}=\frac{\partial\varphi/\partial\theta}{dx/d\theta}=-\frac{2}{\sin\theta}\frac{\partial\varphi}{\partial\theta} \tag{C4}$$

Now according to Watson's equations (10), (24), and (27), in the absence of circulation the values of $\partial\varphi/\partial\theta$ at the points θ_m are given by

$$-\frac{\partial\varphi}{\partial\theta}\bigg)_m=\sum_{p=0}^{2N-1}\beta_p Y_{m+p}, \quad \beta_p=\begin{cases}\frac{1}{2}N, & p=0\\[4pt] 0, & p=\text{even, not }0\\[4pt] -\frac{1}{N(1-\cos\theta_p)}, & p=\text{odd}\end{cases} \tag{C5}$$

Now since $\beta_{2N-p}=\beta_p$ and $Y_0=Y_\pi=0$,

$$\sum_{p=0}^{2N-1}\beta_p Y_{m+p}=\sum_{p=1}^{N-1}\beta_{p-m}Y_p+\sum_{p=1}^{N-1}\beta_{p+m}Y_{2N-p} \tag{C6}$$

Symmetrical airfoils.—For a symmetric airfoil $Y_{2N-s}=-Y_s=-T_s$. Then according to equations (C4), (C5), and (C6)

$$\frac{u_t}{U}\bigg)_m=\sum_{p=1}^{N-1}c_{mp}T_p, \qquad c_{mp}=\frac{2}{\sin\theta_m}(\beta_{p-m}-\beta_{p+m}) \tag{C7}$$

This form is convenient for calculating the c_{mp}. It is also easily shown, using trigonometric identities, that

$$c_{mp}\begin{cases}\dfrac{N}{\sin\theta_m}, & p\pm m=0\\[8pt] 0, & p\pm m=\text{even, not }0\\[8pt] -\dfrac{4\sin\theta_p}{N(\cos\theta_m-\cos\theta_p)^2}, & p\pm m=\text{odd}\end{cases} \tag{C8}$$

which is Weber's result (ref. 24). Corresponding forms can, if desired, be found for the other influence coefficients discussed later.

Antisymmetric airfoils.—For a cambered airfoil of zero thickness $Y_{2N-p}=Y_p=C_p$. Equation (C6) gives

$$\sum_{p=0}^{2N-1}\beta_p Y_{m+p}=\sum_{p=1}^{N-1}(\beta_{p-m}+\beta_{p+m})C_p \tag{C9}$$

This expression represents the velocity on the unit circle into which the airfoil is mapped. The Kutta condition will be violated at the trailing edge of the airfoil unless the expression happens to vanish for $m=0$. Adding a component of circulatory flow changes the velocity on the circle by a constant. Hence the Kutta condition is enforced by subtracting from the expression of equation (C9) its value at $m=0$, so that

$$\sum_{p=0}^{2N-1}\beta_p Y_{m+p}\rightarrow\sum_{p=1}^{N-1}(\beta_{p-m}+\beta_{p+m}-2\beta_p)C_p \tag{C10}$$

Hence, according to equations (C4) and (C5)

$$\frac{u_c}{U}\bigg)=\sum_{p=0}^{N}d_{mp}C_p, \qquad d_{mp}=\frac{2}{\sin\theta_m}(\beta_{p-m}+\beta_{p+m}-2\beta_p) \tag{C11}$$

SLOPE OF AIRFOIL

The airfoil slope is given by

$$Y'\equiv\frac{dY}{dx}=-\frac{2}{\sin\theta}\frac{dY}{d\theta} \tag{C12}$$

Now according to Watson's equations (29), (31), and (34)

$$\frac{dY}{d\theta}\bigg)_m=\sum_{p=0}^{2N-1}\gamma_p Y_{m+p}, \quad \gamma_p=\begin{cases}0, & p=0\\[4pt] -\frac{1}{2}(-1)^p\dfrac{\sin\theta_p}{1-\cos\theta_p}, & p\neq0\end{cases} \tag{C13}$$

or, since $\gamma_{2N-p}=-\gamma_p$

$$\frac{dY}{d\theta}\Big)_m = \sum_{p=1}^{N-1} \gamma_{p-m}Y_p - \sum_{p=1}^{N-1} \gamma_{p+m}Y_{2N-p} \quad \text{(C14)}$$

Symmetric airfoils.—Using the symmetry conditions again gives for symmetric airfoils

$$T'_m = \sum_{p=1}^{N-1} e_{mp}T_p, \qquad e_{mp}=-\frac{2}{\sin\theta_m}(\gamma_{p-m}+\gamma_{p+m}) \quad \text{(C15)}$$

Antisymmetric airfoils.—Similarly, for camber lines

$$C'_m = \sum_{p=1}^{N-1} f_{mp}C_p, \qquad f_{mp}=\frac{2}{\sin\theta_m}(\gamma_{p+m}-\gamma_{p-m}) \quad \text{(C16)}$$

SECOND DERIVATIVE

The second derivative of the airfoil ordinate is given by

$$Y'' \equiv \frac{d^2Y}{dx^2}=\frac{4}{\sin^2\theta}\left(\frac{d^2Y}{d\theta^2}-\cot\theta\,\frac{dY}{d\theta}\right) \quad \text{(C17)}$$

An approximation for $d^2Y/d\theta^2$, which is required here, is found by extending Watson's analysis for the first derivative, as he suggests. Following closely his section 2.4 gives, after some computation,

$$\frac{d^2Y}{d\theta^2}\Big)_m = \sum_{p=0}^{2N-1} \mu_p Y_{m+p}, \quad \mu_p=\begin{cases} -\dfrac{2N^2+1}{6}, & p=0 \\[2mm] -(-1)^p\dfrac{1}{1-\cos\theta_p}, & p\neq 0 \end{cases} \quad \text{(C18)}$$

Symmetric airfoils.—By the foregoing procedure, it is found that for symmetric airfoils

$$T''_m = \sum_{p=1}^{N} g_{mp}Y_p,$$

$$g_{mp}=\frac{4}{\sin^2\theta_m}[(\mu_{p-m}-\mu_{p+m})-\cot\theta_m(\gamma_{p-m}+\gamma_{p+m})] \quad \text{(C19)}$$

Antisymmetric airfoils.—Similarly for camber lines [1]

$$C''_m = \sum_{p=1}^{N-1} h_{mp}Y_p,$$

$$h_{mp}=\frac{4}{\sin^2\theta_m}[(\mu_{p-m}+\mu_{p+m})-\cot\theta_m(\gamma_{p-m}-\gamma_{p+m})] \quad \text{(C20)}$$

EDGE RADII

If the airfoil has round leading and trailing edges, their radii are given by

$$\rho=\lim_{x\to 0} 2xY'^2, \qquad \rho=\lim_{x\to 1} 2(1-x)Y'^2 \quad \text{(C21)}$$

Near the edges, to a first approximation

$$x=\left(\frac{dx}{d\theta}\right)^2, \qquad 1-x=\left(\frac{dx}{d\theta}\right)^2 \quad \text{(C22)}$$

so that

$$\sqrt{\frac{\rho}{2}}=\lim_{\theta\to\pi,0}\frac{dY}{d\theta} \quad \text{(C23)}$$

Setting $m=N$ and 0 in equation (C14) and using the symmetry properties of the thickness and camber distributions gives

$$\sqrt{\frac{\rho}{2}}=-2\sum_{p=1}^{N-1}\gamma_{N-p}T_p, \qquad 2\sum_{p=1}^{N-1}\gamma_p T_p \quad \text{(C24)}$$

at the leading and trailing edges, respectively.

SLOPE OF CAMBER LINE AT END

Equation (C16) is indeterminate at the ends of the airfoil. Applying L'Hospital's rule to equation (C12) gives at $\theta=0$

$$Y_0'=-2\frac{d^2Y}{d\theta^2} \quad \text{(C25)}$$

Then using equation (C18) and the fact that $Y_{2N-p}=Y_p=C_p$ for a camber line gives

$$Y_0'=-\sum_1^{N-1}f_pC_p, \qquad f_p\equiv f_{op}=-4(-1)^b\frac{1}{1-\cos\theta_p} \quad \text{(C26)}$$

ANGLE-OF-ATTACK PARAMETER α

The parameter a is the coefficient of the square-root leading-edge singularity in the surface speed. There is a first-order contribution from u_{1c}/U (eq. (4)), and second-order contributions from u_{2c}/U (eq. (8)) and $(C\pm T)(C''\pm T'')+1/2(C'\pm T')^2$ (eq. (9)).

For zero angle of attack, equations (C4), (C5), and (C10) give

$$\frac{u_c}{U}=\frac{2}{|\sin\theta|}\sum_{p=1}^{N-1}(\beta_{p-m}+\beta_{p+m}-2\beta_p)C_p \quad \text{(C27)}$$

Near the leading edge

$$\sin\theta\sim\sqrt{2x} \quad \text{(C28)}$$

so that (since $\beta_{p-N}=\beta_{p+N}=\beta_{N-p}$)

$$\frac{u_c}{U}\sim 2\sqrt{\frac{2}{x}}\sum_{p=1}^{N-1}(\beta_{N-p}-\beta_p)C_p \quad \text{(C29)}$$

Including the contribution of angle of attack from equation (4) gives for the first-order approximation to a

$$a_1=\sqrt{2}\left(\alpha+\sum_{p=1}^{N-1}d_pC_p\right), \quad d_p=2(\beta_{N-p}-\beta_p) \quad \text{(C30)}$$

For a round nose described by equation (15a), the terms $(C\pm T)(C''\pm T'')+1/2(C'\pm T')^2$ of equation (9) contribute.

$$\frac{1}{2}\lambda\sqrt{\frac{\rho}{2}}x^{-1/2}$$

Hence the second-order increment in a is

$$\Delta a_2=\sqrt{2}\sum_{p=1}^{N-1}d_pC_{2p}+\frac{1}{2}\lambda\sqrt{\frac{\rho}{2}} \quad \text{(C31)}$$

---

[1] The expression given for μ_p in NACA TN 3390 is incorrect, differing from that of the present equation (C18) by $1/2(-1)^pN$. The error cancels out in the g_{mp}, but the values of h_{mp} tabulated there are affected. However, the correction has little effect (except to simplify the tables) since the approximation merely becomes exact for the first 8 Fourier components rather than the first 7 (in the case $N=8$).

TABLES

The various influence coefficients have been calculated for $N=8$ and $N=16$. The values have been checked by applying them to a number of simple shapes—ellipse, parabolic arc camber line, etc.—for which the approximation of the airfoil by a trigonometric polynomial is exact. They were also checked against Weber's values (refs. 24 and 25) where possible. The values are believed to be accurate to within one unit in the last place.

For convenience of computation, the coefficients have been renumbered so that the pivotal points are counted from the leading to the trailing edge. This renumbering is indicated by using indices (n, s) instead of (m, p). The above results are formally unchanged, except that the roles of leading and trailing edge are interchanged in equation (C24), the sign of equation (C26) is reversed, and the sign of d_p is reversed (eq. (C30)). The renumbered influence coefficients are given in tables I to IV.

REFERENCES

1. Riegels, F., and Wittich, H.: Zur Berechnung der Druckverteilung von Profilen. Jan. 24, 1942. Aerodynamische Versuchsanstalt Göttingen E. V. Institut für theoretische Aerodynamik. Bericht 41/1/15.
2. Riegels, F.: Das Umströmungsproblem bei inkompressiblen Potentialströmungen. Ing.-Archiv., Bd. XVI, 1948, pp. 373–376, and Bd. XVII, 1949, pp. 94–106.
3. Keune, F.: Beiträge zur Profilforschung. VI. Zweite Näherung zur Berechnung der Geschwindigkeitsverteilung nach dem Singularitätenverfahren. Luftfahrtforschung, Bd. 20, Lfg. 6, June 1943, pp. 196–206.
4. Goldstein, Sydney: Low-drag and Suction Airfoils. Jour. Aero. Sci., vol. 15, no. 4, Apr. 1948, pp. 189–214.
5. Lighthill, M. J.: A New Approach to Thin Aerofoil Theory. Aero Quart., vol. 3, pt. 3, Nov. 1951, pp. 193–210.
6. Görtler, H.: Gasströmungen mit Übergang von Unterschall- zu Überschallgeschwindigkeiten. Z. a. M. M., Bd. 20, Heft 5, Oct. 1940, pp. 254–262.
7. Hantzsche, W., and Wendt, H.: Der Kompressibilitätseinfluss für dünne wenig gekrümmte Profile bei Unterschallgeschwindigkeit. Z. a. M. M., Bd. 22, Nr. 2, Apr. 1942, pp. 72–86.
8. Hantzsche, W.: Die Prandtl-Glauertsche Näherung als Grundlage für ein iterationsverfahren zur Berechnung kompressibler Unterschallströmungen. Z. a. M. M., Bd. 23, Heft 4, Aug. 1943, pp. 185–199.
9. Schmieden, C., and Kawalki, K. H.: Beiträge zum Umströmungsproblem bei hohen Geschwindigkeiten. Bericht S13, Teil 1, L. G. L., 1942, pp. 40–68. (Available in translation as NACA TM 1233, 1949.)
10. Kaplan, Carl: The Flow of a Compressible Fluid Past a Curved Surface. NACA Rep. 768, 1943.
11. Kaplan, Carl: The Flow of a Compressible Fluid Past a Circular Arc Profile. NACA Rep. 794, 1944.
12. Imai, Isao: Two-Dimensional Aerofoil Theory for Compressible Fluids. Rep. No. 294 (vol. 21, no. 9), Aero. Res. Inst., Tokyo Imperial Univ., May 1944, pp. 283–331. (Japanese text with English abstract.)
13. Imai, Isao, and Oyama, Seiichi: The Third Approximation of the Thin-Wing Expansion Method for Compressible Fluids. Repts. Inst. of Sci. and Tech., Univ. Tokyo, vol. 2, nos. 3–4, Mar.–Apr. 1948, pp. 33–44. (Japanese text)
14. Van Dyke, Milton D.: A Study of Second-Order Supersonic Flow Theory. NACA Rep. 1081, 1952.
15. Keune, Friedrich: Das Tragflügel-Profil in der ebenen inkompressiblen und kompressiblen Strömung. Rapport FI 12, FI 13, Flygtekniska Institutionen, Kungl. Tekniska Högskolan, Stockholm, Feb.–May 1951.
16. Harder, Keith C., and Klunker, E. B.: On a Source-Sink Method for the Solution of the Prandtl-Busemann Iteration Equations in Two-Dimensional Compressible Flow. NACA TN 2253, 1950.
17. Hayes, Wallace D.: Second-Order Pressure Law for Two-Dimensional Compressible Flow. Jour. Aero. Sci., vol. 22, no. 4, April 1955, pp. 284–286. (Originally published as: Second-Order Two-Dimensional Flow Theory and Imai's Similitude. British A. R. C. 15,722, F. M. 1877, 1953.)
18. Imai, Isao: Extension of von Kármán's Transonic Similarity Rule. Jour. Phys. Soc. Japan, vol. 9, no. 1, Jan.–Feb. 1954, pp. 103–108.
19. Van Dyke, Milton D.: The Second-Order Compressibility Rule for Airfoils. Jour. Aero. Sci., vol. 21, no. 9, Sept. 1954, pp. 647–648.
20. Van Dyke, Milton D.: Subsonic Edges in Thin-Wing and Slender-Body Theory. NACA TN 3343, 1954.
21. Germain, P.: Sur le calcul numérique de certains opérateurs linéaires. Comptes Rendes Aca. Sci. Paris, vol. 220, 1945, pp. 765–768.
22. Watson, E. J.: Formulae for the Computation of the Functions Employed for Calculating the Velocity Distribution about a Given Aerofoil. R. & M. No. 2176, British A. R. C., 1945.
23. Thwaites, B.: A Method of Aerofoil Design. Part I—Symmetrical Aerofoils. R. & M. No. 2166, British A. R. C., 1945.
24. Weber, J.: The Calculation of the Pressure Distribution over the Surface of Two-Dimensional and Swept Wings with Symmetrical Aerofoil Sections. R. A. E. Rep. Aero. 2497, 1953.
25. Weber, J.: The Calculation of the Pressure Distribution on the Surface of Thick Cambered Wings and the Design of Wings With Given Pressure Distributions. British R. A. E. Rept. Aero. 2548, June, 1955.
26. Munk, Max M.: Elements of the Wing Section Theory and of the Wing Theory. NACA Rep. 191, 1924.
27. Pistolesi, E.: Sulla Teoria delle Ali Sottili. Acta Pont. Acad. Sci., vol. 1, 1937, pp. 57–72.
28. Goldstein, Sydney: Approximate Two-Dimensional Aerofoil Theory. Part I. Velocity Distributions for Symmetrical Aerofoils. C. P. 68, British A. R. C., 1942.
29. Jones, Robert T., and Cohen, Doris: Aerodynamics of Wings at High Speeds. Section A of vol. VII, Aerodynamic Components of Aircraft at High Speeds, High-Speed Aerodynamics and Jet Propulsion. Princeton Univ. Press, 1957.
30. Erdélyi, A., ed.: Tables of Integral Transforms, vol. 2, ch. 15. McGraw-Hill, 1954.
31. Imai, Isao: Application of the M^2-Expansion Method to the Subsonic Flow of a Compressible Fluid Past a Parabolic Cylinder. Proc. 1st Japan Nat. Cong. Appl. Mech., 1952, pp. 349–352.
32. Kaplan, Carl: On the Small-Disturbance Iteration Method for the Flow of a Compressible Fluid With Application to a Parabolic Cylinder. NACA TN 3318, 1955.
33. Kaplan, Carl: On the Use of Residue Theory for Treating the Subsonic Flow of a Compressible Fluid. NACA Rep. 728, 1942.
34. Allen, H. Julian: General Theory of Airfoil Sections Having Arbitrary Shape or Pressure Distribution. NACA Rep. 833, 1945.
35. Milne-Thomson, L. M.: Theoretical Hydrodynamics. Second ed., Macmillan Co., 1949.
36. Jacobs, Eastman N., Ward, Kenneth E., and Pinkerton, Robert M.: The Characteristics of 78 Related Airfoil Sections from Tests in the Variable-Density Wind Tunnel. NACA Rep. 460, 1933.
37. Goldstein, S.: Notes on "General Theory of Airfoil Sections Having Arbitrary Shape or Pressure Distribution," by H. Julian Allen. British A. R. C. Rep. No. 7142, F. M. 624, 1943.
38. Abbott, Ira H., Von Doenhoff, Albert E., and Stivers, Louis S., Jr.: Summary of Airfoil Data. NACA Rep. 824, 1945.
39. Hasimoto, H.: Application of the Thin-Wing Expansion Method to the Compressible Flow Past an Elliptic Cylinder. Jour. Phys. Soc. Japan, vol. 7, no. 3, 1952, pp. 322–328.

40. Emmons, Howard W.: Flow of a Compressible Fluid Past a Symmetrical Airfoil in a Wind Tunnel and in Free Air. NACA TN 1746, 1948.

41. Graham, Donald J., Nitzberg, Gerald E., and Olsen, Robert N.: A Systematic Investigation of Pressure Distributions at High Speeds over Five Representative NACA Low-Drag and Conventional Airfoil Sections. NACA Rep. 832, 1945.

42. Tomotika, S., and Tamada, K.: Studies on Two-Dimensional Transonic Flows of Compressible Fluid. Part III. Quart. Appl. Math., vol. 9, July 1951, pp. 129–147.

43. Asaka, Saburô: Application of the Thin-Wing-Expansion Method to the Flow of a Compressible Fluid Past a Symmetrical Circular Arc Aerofoil. Jour. Phys. Soc. Japan, vol. 10, no. 6, 1955, pp. 482–492.

TABLE I.—PIVOTAL POINTS, INCLINED FLAT PLATE SOLUTION, AND INFLUENCE COEFFICIENTS FOR ρ, λ, a

$N=8$

n	x_n	$\sqrt{\dfrac{1-x_n}{x_n}}$	r_n (for $\sqrt{\rho/2}$)	f_n (for λ)	d_n (for a)
1	0.03806	5.0273	5.0273	52.5483	-3.1543
2	.14645	2.4142	-2.4142	-13.6569	0
3	.30865	1.4966	1.4966	6.4797	-.2242
4	.50000	1.0000	-1.0000	-4.0000	0
5	.69134	.6682	.6682	2.8929	.2242
6	.85355	.4142	-.4142	-2.3431	0
7	.96194	.1989	.1989	2.0791	3.1543

$N=16$

n	x_n	$\sqrt{\dfrac{1-x_n}{x_n}}$	r_n (for $\sqrt{\rho/2}$)	f_n (for λ)	d_n (for a)
1	0.00961	10.1532	10.1532	208.174	-6.4423
2	.03806	5.0273	-5.0273	-52.548	0
3	.08426	3.2966	3.2966	23.735	-.6735
4	.14645	2.4142	-2.4142	-13.657	0
5	.22222	1.8709	1.8709	9.000	-.2009
6	.30866	1.4966	-1.4966	-6.480	0
7	.40246	1.2185	1.2185	4.970	-.0507
8	.50000	1.0000	-1.0000	-4.000	0
9	.59754	.8207	.8207	3.347	.0507
10	.69134	.6682	-.6682	-2.893	0
11	.77778	.5345	.5345	2.571	.2009
12	.85355	.4142	-.4142	-2.343	0
13	.91574	.3033	.3033	2.184	.6735
14	.96194	.1989	-.1989	-2.079	0
15	.99039	.0985	.0985	2.019	6.4423

TABLE II.—INFLUENCE COEFFICIENTS FOR VELOCITY (a) $N=8$

c_{ns} (velocity due to thickness)

s \ n	1	2	3	4	5	6	7
1	20.9050	-4.0719	0	-0.2242	0	-0.0719	0
2	-7.5240	11.3137	-3.3592	0	-.2977	0	-.1329
3	0	-4.3890	8.6591	-3.1543	0	-.3890	0
4	-.5858	0	-3.4142	8.0000	-3.4142	0	-.5858
5	0	-.3890	0	-3.1543	8.6591	-4.3890	0
6	-.1329	0	-.2977	0	-3.3592	11.3137	-7.5240
7	0	-.0719	0	-.2242	0	-4.0719	20.9050

d_{ns} (velocity due to camber)

s \ n	1	2	3	4	5	6	7
1	21.5841	-4.8498	0.2813	-0.3259	0.2813	-0.0719	0.6791
2	-9.6405	11.3137	-3.7506	0	-.5790	0	-.8120
3	.9450	-4.3890	9.0506	-3.0526	.3914	-.2451	.9450
4	-1.5307	0	-3.6955	8.0000	-3.6955	0	-1.5307
5	2.1165	.3890	.8767	-2.6043	9.5358	-3.7549	2.1165
6	-.8120	0	-.5790	0	-3.7506	11.3137	-9.6405
7	17.1644	8.8498	7.1097	5.9828	7.1097	4.0719	38.0694

(b) $N=16$

c_{ns} (velocity due to thickness)

s \ n	1	2	3	4	5	6	7	8	9	10	11	12	13	14	15
1	82.0133	-15.0614	0	-0.6512	0	-0.1363	0	-0.0507	0	-0.0262	0	-0.0171	0	0.0134	0
2	-29.5439	41.8100	-11.2032	0	-.7053	0	-.1801	0	-.0764	0	-.0437	0	-.0310	0	-.0264
3	0	-16.2646	23.7992	-8.9804	0	-.6896	0	-.2009	0	-.0942	0	-.0587	0	-.0451	0
4	-2.3602	0	-11.4300	22.6274	-9.0522	0	-.6743	0	-.2172	0	-.1109	0	-.0747	0	-.0620
5	0	-1.5324	0	-9.0522	19.2430	-7.7274	0	-.6735	0	-.2361	0	-.1304	0	-.0950	0
6	-.6457	0	-1.1468	0	-7.7274	17.3183	-6.5633	0	-.6919	0	-.2624	0	-.1567	0	-.1242
7	0	-.4616	0	-.9353	0	-6.9676	16.3135	-6.4423	0	-.7345	0	-.3012	0	-.1958	0
8	-.2599	0	-.3616	0	-.6972	0	-6.4423	16.0000	-6.4423	0	-.6972	0	-.3616	0	-.2599
9	0	-.1958	0	-.3012	0	-.7345	0	-6.4423	16.3135	-6.9676	0	-.9353	0	-.4616	0
10	-.1242	0	-.1567	0	-.2624	0	-.6919	0	-6.5633	17.3183	-7.7274	0	-1.1468	0	-.6457
11	0	-.0950	0	-.1304	0	-.2361	0	-.6735	0	-7.7274	19.2430	-9.0522	0	-1.5324	0
12	-.0620	0	-.0747	0	-.1109	0	-.2172	0	-.6743	0	-9.0522	22.6274	-11.4300	0	-2.3602
13	0	-.0451	0	-.0587	0	-.0942	0	-.2009	0	-.6896	0	-8.9804	23.7992	-16.2646	0
14	-.0264	0	-.0310	0	-.0437	0	-.0764	0	-.1801	0	-.7053	0	-11.2032	41.8100	-29.5439
15	0	.0134	0	-.0171	0	-.0262	0	-.0507	0	-.1363	0	-.6512	0	-15.0614	82.0133

d_{ns} (velocity due to camber)

s \ n	1	2	3	4	5	6	7	8	9	10	11	12	13	14	15
1	82.6602	-18.6079	0.2272	-1.2682	0.1518	-0.3359	0.1287	-0.1337	0.1286	-0.0638	0.1518	-0.0317	0.2272	-0.0134	0.6469
2	-37.1476	41.8100	-12.2157	0	-1.0788	0	-.3934	0	-.2403	0	-.2079	0	-.2582	0	-.6733
3	.6997	-17.3778	29.0449	-9.2267	.2893	-.7683	.1642	-.2251	.1392	-.0942	.1642	-.3018	.2893	-.2457	-.6997
4	-5.2436	0	-11.9890	22.6274	-9.1207	0	-.8382	0	-.3564	0	-.2627	0	1.8607	0	-.7617
5	.8238	-1.9240	.2893	-7.9498	19.4363	-7.9207	.1639	-.6492	.1639	-.1988	.1933	-.2627	1.7841	-.2079	-.8238
6	-2.2377	0	-1.5233	0	-7.9207	17.3183	-6.7025	0	-.8206	0	-.4142	0	1.3637	0	-.9480
7	1.0723	-.4616	.3765	-.8667	.2516	-6.8889	16.5267	-6.5394	.2133	-.6447	.2516	-.3564	1.5125	-.2403	1.0723
8	-1.3322	0	-.6509	0	-.9741	0	-6.6972	16.0000	-6.6972	0	-.9741	0	1.1218	0	-1.3322
9	1.5920	.1958	.5590	-.0550	.3736	-.5349	.3167	-6.6972	16.6301	-6.7025	.5735	-.8382	1.5125	-.3934	1.5920
10	-.9480	0	-.4024	0	-.4142	0	-.8206	0	-6.7025	17.3183	-7.9498	0	.6896	0	-2.2377
11	2.8834	1.0183	1.0125	.4866	.6765	.2361	.5735	-.2474	.5735	-7.9498	19.9196	-7.9498	1.7841	-1.0788	2.8834
12	-.7617	0	-.3018	0	-.2627	0	-.3564	0	-.8382	0	-7.9498	22.6274	-12.2147	0	-5.2436
13	7.6037	3.5015	2.6701	1.8607	1.7841	1.3637	1.5125	1.1218	1.5125	.6896	1.7841	-12.2147	31.4693	-13.8582	7.6037
14	-.6733	-.2582	-.2582	0	-.2079	0	-.2403	0	-.3934	0	-1.0788	0	-13.8582	41.8100	-37.1476
15	66.6915	33.6558	23.4190	18.1900	15.6480	13.8827	13.2658	12.7510	13.2658	13.6103	15.6480	16.9535	23.4190	15.0614	148.7048

TABLE III.—INFLUENCE COEFFICIENTS FOR SLOPE

(a) $N=8$

e_{ns} (slope due to thickness)

$s \backslash n$	1	2	3	4	5	6	7
1	−6.3086	−4.9932	1.5307	−0.8284	0.6340	−0.6636	1.0824
2	17.0479	−1.4142	−4.7183	2.0000	−1.4046	1.4142	−2.2058
3	−8.9218	8.0547	−.4483	−4.8284	2.6131	−2.3978	3.6955
4	5.6568	−4.0000	5.6568	0	−5.6568	4.0000	−5.6568
5	−3.6955	2.3978	−2.6131	4.8284	.4483	−8.0547	8.9218
6	2.2658	−1.4142	1.4046	−2.0000	4.7183	1.4142	−17.0479
7	−1.0824	.6636	−.6340	.8284	−1.5307	4.9932	6.3086

f_{ns} (slope due to camber)

$s \backslash n$	1	2	3	4	5	6	7
1	6.3086	−9.2262	3.6955	−2.1648	1.5307	−1.2262	1.0824
2	9.2262	1.4142	−6.1648	2.8284	−1.8352	1.4142	−1.2262
3	−3.6955	6.1648	.4483	−5.2262	2.6131	−1.8352	1.5307
4	2.1648	−2.8284	5.2262	0	−5.2262	2.8284	−2.1648
5	−1.5307	1.8352	−2.6131	5.2262	−.4483	−6.1648	3.6955
6	1.2262	−1.4142	1.8352	−2.8284	6.1648	−1.4142	−9.2262
7	−1.0824	1.2262	−1.5307	2.1648	−3.6955	9.2262	−6.3086

(b) $N=16$

e_{ns} (slope due to thickness)

$s \backslash n$	1	2	3	4	5	6	7	8	9	10	11	12	13	14	15
1	−25.7693	−17.9172	4.7035	−2.0162	1.1036	−0.7061	0.5063	−0.3978	0.3383	−0.3098	0.3054	−0.3269	0.3875	−0.5353	1.0196
2	68.9411	−6.3086	−14.9078	4.9932	−2.4992	1.5307	−1.0708	.8284	−.6974	.6340	−.6222	.6636	−.7848	1.0824	−2.0598
3	−38.1441	31.4204	−2.6938	−12.6356	4.8436	−2.6799	1.7802	−1.3364	1.1036	−.9906	.9635	−1.0213	1.2027	−1.6541	3.1428
4	26.4874	−17.0479	20.4685	−1.4142	−11.2241	4.7183	−2.8162	2.0000	−1.5982	1.4046	−1.3470	1.4142	−1.6545	2.2658	−4.2947
5	−20.0462	11.7384	−10.8489	15.5194	−.8036	−10.4112	4.7035	−2.9932	2.2587	−1.9184	1.8000	−1.8625	2.1580	−2.9372	5.5482
6	15.8356	−8.9218	7.4108	−8.0547	12.8540	−.4483	−10.0428	4.8284	−3.2607	2.6131	−2.3685	2.3978	−2.7393	3.6955	−6.9465
7	−12.7972	7.0334	−5.5482	5.4180	−6.5445	11.3181	−.2028	−10.0547	5.1258	−3.6748	3.1428	−3.0748	3.4394	−4.5808	8.5508
8	10.4525	−5.6568	4.3296	−4.0000	4.3296	−5.6568	10.4525	0	−10.4525	5.6568	−4.3296	4.0000	−4.3296	5.6568	−10.4525
9	−8.5508	4.5808	−3.4394	3.0748	−3.1428	3.6748	−5.1258	10.0547	.2028	−11.3181	6.5445	−5.4180	5.5482	−7.0334	12.7972
10	6.9465	−3.6955	2.7393	−2.3978	2.3685	−2.6131	3.2607	−4.8284	10.0428	.4483	−12.8540	8.0547	−7.4108	8.9218	−15.8356
11	−5.5482	2.9372	−2.1580	1.8625	−1.8000	1.9184	−2.2587	2.9932	−4.7035	10.4112	.8036	−15.5194	10.8489	−11.7384	20.0462
12	4.2947	−2.2658	1.6545	−1.4142	1.3470	−1.4046	1.5982	−2.0000	2.8162	−4.7183	11.2241	1.4142	−20.4685	17.0479	−26.4874
13	−3.1428	1.6541	−1.2027	1.0213	−.9635	.9906	−1.1036	1.3364	−1.7802	2.6799	−4.8436	12.6356	2.6938	−31.4204	38.1441
14	2.0598	−1.0824	.7848	−.6636	.6222	−.6340	.6974	−.8284	1.0708	−1.5307	2.4992	−4.9932	14.9078	6.3086	−68.9411
15	−1.0196	.5353	−.3875	.3269	−.3054	.3098	−.3383	.3978	−.5063	.7061	−1.1036	2.0162	−4.7035	17.9172	25.7693

f_{ns} (slope due to camber)

$s \backslash n$	1	2	3	4	5	6	7	8	9	10	11	12	13	14	15
1	25.7693	−35.1459	13.3944	−7.3078	4.7035	−3.3439	2.5455	−2.0392	1.7009	−1.4668	1.3018	−1.1849	1.1036	−1.0500	1.0196
2	35.1459	6.3086	−21.6427	9.2262	−5.4302	3.6955	−2.7443	2.1648	−1.7874	1.5307	−1.3518	1.2262	−1.1394	1.0824	−1.0500
3	−13.3944	21.6427	2.6938	−16.0820	7.2490	−4.4565	3.1428	−2.4054	1.9482	−1.6472	1.4419	−1.2999	1.2027	−1.1394	1.1036
4	7.3078	−9.2262	16.0820	1.4142	−13.1982	6.1648	−3.9061	2.8284	−2.2168	1.8352	−1.5839	1.4142	−1.2999	1.2262	−1.1849
5	−4.7035	5.4302	−7.2490	13.1982	.8036	−11.5683	5.5482	−3.5999	2.6643	−2.1316	1.8000	−1.5839	1.4419	−1.3518	1.3018
6	3.3439	−3.6955	4.4565	−6.1648	11.5683	.4483	−10.6614	5.2262	−3.4616	2.6131	−2.1316	1.8352	−1.6472	1.5307	−1.4669
7	−2.5455	2.7443	−3.1428	3.9061	−5.5482	10.6614	.2028	−10.2517	5.1258	−3.4616	2.6643	−2.2168	1.9482	−1.7874	1.7009
8	2.0392	−2.1648	2.4054	−2.8284	3.5999	−5.2262	10.2517	0	−10.2517	5.2262	−3.5999	2.8284	−2.4054	2.1648	−2.0392
9	−1.7009	1.7874	−1.9482	2.2168	−2.6643	3.4616	−5.1258	10.2517	−.2028	−10.6614	5.5482	−3.9061	3.1428	−2.7443	2.5455
10	1.4669	−1.5307	1.6472	−1.8352	2.1316	−2.6131	3.4616	−5.2262	10.6614	−.4483	−11.5683	6.1648	−4.4565	3.6955	−3.3439
11	−1.3018	1.3518	−1.4419	1.5839	−1.8000	2.1316	−2.6643	3.5999	−5.5482	11.5683	−.8036	−13.1982	7.2490	−5.4302	4.7035
12	1.1849	−1.2262	1.2999	−1.4142	1.5839	−1.8352	2.2168	−2.8284	3.9061	−6.1648	13.1982	−1.4142	−16.0820	9.2262	−7.3078
13	−1.1036	1.1394	−1.2027	1.2999	−1.4419	1.6472	−1.9482	2.4054	−3.1428	4.4565	−7.2490	16.0820	−2.6938	−21.6427	13.3944
14	1.0500	−1.0824	1.1394	−1.2262	1.3518	−1.5307	1.7874	−2.1648	2.7443	−3.6955	5.4302	−9.2262	21.6427	−6.3086	−35.1459
15	−1.0196	1.0500	−1.1036	1.1849	−1.3018	1.4668	−1.7009	2.0392	−2.5455	3.3439	−4.7035	7.3078	−13.3944	35.1459	−25.7693

TABLE IV.—INFLUENCE COEFFICIENTS FOR SECOND DERIVATIVE

(a) N=8

g_{sn} (second derivative due to thickness)

s\n	1	2	3	4	5	6	7
1	−414.392	106.260	−12.686	3.587	−1.373	−0.250	11.314
2	99.478	−160.000	62.406	−11.314	3.896	0	−23.032
3	46.627	76.529	−97.608	50.469	−11.314	2.019	35.314
4	−46.882	−11.314	54.056	−84.000	54.056	−11.314	−46.882
5	35.314	2.019	−11.314	50.469	−97.608	76.529	46.627
6	−23.032	0	3.896	−11.314	62.406	−160.000	99.478
7	11.314	−.250	−1.373	3.587	−12.686	106.260	−414.392

h_{sn} (second derivative due to camber)

s\n	1	2	3	4	5	6	7
1	−760.098	144.152	−24.000	9.373	−6.059	6.476	−16.000
2	286.658	−184.000	70.481	−16.000	8.382	−8.000	18.479
3	−73.941	93.446	−103.902	54.627	−16.000	11.927	−24.000
4	36.686	−104.000	59.314	−88.000	59.314	−104.000	36.686
5	−24.000	11.927	−16.000	54.627	−103.902	93.446	−73.941
6	18.479	−8.000	8.382	−16.000	70.481	−184.000	286.658
7	−16.000	6.476	−6.059	9.373	−24.000	144.152	−760.098

(b) N=16

g_{sn} (second derivative due to thickness)

s\n	1	2	3	4	5	6	7	8	9	10	11	12	13	14	15
1	−6276.99	1485.50	−151.34	35.17	−12.16	5.36	−2.78	1.62	−1.01	0.63	−0.36	−0.15	1.23	−5.63	50.47
2	1292.86	−2162.47	725.61	−106.26	31.16	−12.69	6.31	−3.59	2.21	−1.37	.68	.25	−2.44	11.31	−101.83
3	944.06	963.60	−1072.52	442.15	−78.01	26.29	−11.91	6.43	−3.85	2.38	−1.23	−.23	3.59	−17.10	155.04
4	−977.99	−99.48	548.07	−672.00	314.31	−63.41	23.14	−11.31	6.44	−3.90	2.10	0	−4.61	23.03	−211.17
5	844.58	−20.73	−98.84	365.76	−489.21	250.21	−54.10	21.55	−11.12	6.46	−3.59	.63	5.40	−29.12	271.50
6	−710.24	46.63	26.13	−76.53	276.74	−397.53	218.21	−50.47	21.25	−11.31	6.29	−2.02	−5.73	35.31	−337.63
7	594.40	−50.14	−4.98	27.00	−62.10	231.18	−353.29	206.15	−50.47	22.15	−11.70	4.94	5.13	−41.42	411.61
8	−496.08	46.88	−2.50	−11.31	24.21	−54.06	210.07	−340.00	210.07	−54.06	24.21	−11.31	−2.50	46.88	−496.08
9	411.61	−41.42	5.13	4.94	−11.70	22.15	−50.47	206.15	−353.29	231.18	−62.10	27.00	−4.98	−50.14	594.40
10	−337.63	35.31	−5.73	−2.02	6.29	−11.31	21.25	−50.47	218.21	−397.53	276.74	−76.53	26.13	46.63	−710.24
11	271.50	−29.12	5.40	.63	−3.59	6.46	−11.12	21.55	−54.10	250.21	−489.21	365.76	−98.84	−20.73	844.58
12	−211.17	23.03	−4.61	0	2.10	−3.90	6.44	−11.31	23.14	−62.41	314.31	−672.00	548.07	−99.48	−977.99
13	155.04	−17.10	3.59	−.23	−1.23	2.38	−3.85	6.43	−11.91	26.29	−78.01	442.15	−1072.52	963.60	944.06
14	−101.83	11.31	−2.44	.25	.68	−1.37	2.21	−3.59	6.31	−12.69	31.16	−106.26	725.61	−2162.47	1292.86
15	50.47	−5.63	1.23	−.15	−.36	.63	−1.01	1.62	−2.78	5.36	−12.16	35.17	−151.34	1485.50	−6276.99

h_{sn} (second derivative due to camber)

s\n	1	2	3	4	5	6	7	8	9	10	11	12	13	14	15
1	−11694.53	2027.02	−286.66	86.14	−36.69	19.36	−11.93	8.32	−6.48	5.62	−5.48	6.16	−8.38	15.45	−54.63
2	4281.83	−2508.18	820.21	−144.15	50.25	−24.00	13.95	−9.37	7.11	−6.03	5.83	−6.48	8.73	−16.00	56.32
3	−1019.15	1209.89	−1143.53	471.77	−93.45	35.72	−18.48	11.57	−8.38	6.90	−6.48	7.06	−9.37	16.97	−59.31
4	483.45	−286.66	603.90	−696.00	327.17	−70.48	28.93	−16.00	10.73	−8.38	7.56	−8.00	10.38	−18.48	63.88
5	−286.66	127.49	−144.15	385.71	−500.17	257.28	−59.31	25.92	−15.28	11.00	−9.37	9.50	−11.93	20.71	−70.48
6	194.70	−73.94	63.73	−93.45	286.24	−403.83	223.01	−54.63	25.37	−16.00	12.51	−11.93	14.30	−24.00	79.90
7	−144.15	49.69	−36.69	41.56	−70.48	236.89	−357.78	214.35	−54.63	27.07	−18.48	16.10	−18.09	28.94	−93.45
8	113.41	−36.69	24.53	−24.00	31.70	−59.31	214.35	−344.00	214.35	−59.31	31.70	−24.00	24.53	−36.69	113.41
9	−93.45	28.94	−18.09	16.10	−18.48	27.07	−54.63	210.19	−357.78	236.89	−70.48	41.56	−36.69	49.69	−144.15
10	79.90	−24.00	14.30	−11.93	12.51	−16.00	25.37	−54.63	223.01	−403.83	286.24	−93.45	63.73	−73.94	194.70
11	−70.48	20.71	−11.93	9.50	−9.37	11.00	−15.28	25.92	−59.31	257.28	−500.17	385.71	−144.15	127.49	−286.66
12	63.88	−18.48	10.38	−8.00	7.56	−8.38	10.73	−16.00	28.93	−70.48	327.17	−696.00	603.90	−286.66	483.45
13	−59.31	16.97	−9.37	7.06	−6.48	6.90	−8.38	11.57	−18.48	35.72	−93.45	471.77	−1143.53	1209.89	−1019.15
14	56.32	−16.00	8.73	−6.48	5.83	−6.06	7.11	−9.37	13.95	−24.00	50.25	−144.15	820.21	−2508.18	4281.83
15	−54.63	15.45	−8.38	6.16	−5.48	5.62	−6.48	8.32	−11.93	19.36	−36.69	86.14	−286.66	2027.02	−11694.53

TABLE V.—COMPRESSIBILITY FACTORS ($\gamma = 7/5$)

M	K_1	K_2	K_2-1	$\frac{K_2-1}{2}$	M	K_1	K_2	K_2-1	$\frac{K_2-1}{2}$	M	K_1	K_2	K_2-1	$\frac{K_2-1}{2}$
0	1.0000	1.0000	0	0	0.56	1.2070	1.5821	0.58212	0.29106	0.76	1.5386	3.4893	2.4893	1.2447
.05	1.0013	1.0025	.00251	.00126	.57	1.2171	1.6202	.62023	.31012	.77	1.5673	3.7291	2.7291	1.3645
.10	1.0050	1.0102	.01016	.00508	.58	1.2276	1.6611	.66112	.33056	.78	1.5980	4.0019	3.0019	1.5009
.15	1.0114	1.0233	.02334	.01167	.59	1.2385	1.7051	.70506	.35253	.79	1.6310	4.3142	3.3142	1.6571
.20	1.0206	1.0427	.04271	.02135	.60	1.2500	1.7523	.75234	.37617	.80	1.6667	4.6741	3.6741	1.8370
.25	1.0328	1.0693	.06933	.03467	.61	1.2620	1.8033	.80332	.40166	.81	1.7052	5.0917	4.0917	2.0458
.30	1.0483	1.1048	.10477	.05238	.62	1.2745	1.8584	.85838	.42919	.82	1.7471	5.5802	4.5802	2.2901
.35	1.0675	1.1513	.15129	.07565	.63	1.2877	1.9180	.91796	.45898	.83	1.7929	6.1585	5.1585	2.5783
.40	1.0911	1.2122	.21224	.10612	.64	1.3014	1.9826	.98255	.49128	.84	1.8430	6.8434	5.8434	2.9217
.45	1.1198	1.2926	.29260	.14630	.65	1.3159	2.0527	1.0527	.52637	.85	1.8993	7.6708	6.6708	3.3354
.46	1.1262	1.3116	.31161	.15581	.66	1.3311	2.1292	1.1292	.56460	.86	1.9597	8.6804	7.6894	3.8402
.47	1.1329	1.3318	.33177	.16588	.67	1.3471	2.2126	1.2126	.60632	.87	2.0702	9.9300	8.9300	4.4650
.48	1.1399	1.3532	.35315	.17658	.68	1.3639	2.3040	1.3040	.65200	.88	2.1054	11.502	10.502	5.2512
.49	1.1472	1.3759	.37586	.18793	.69	1.3816	2.4043	1.4043	.70213	.89	2.1932	13.520	12.520	6.2598
.50	1.1547	1.4000	.40000	.20000	.70	1.4003	2.5146	1.5146	.75732	.90	2.2942	16.168	15.168	7.5839
.51	1.1626	1.4257	.42568	.21284	.71	1.4200	2.6365	1.6365	.81827	.91	2.4110	19.741	18.741	9.3707
.52	1.1707	1.4530	.45303	.22651	.72	1.4410	2.7716	1.7716	.88580	.92	2.6184	24.729	23.729	11.865
.53	1.1792	1.4822	.48218	.24109	.73	1.4632	2.9218	1.9218	.96091	.93	2.7206	31.993	30.993	15.496
.54	1.1881	1.5133	.51330	.25665	.74	1.4868	3.0895	2.0895	1.0448	.94	3.0196	43.166	42.166	21.083
.55	1.1974	1.5465	.54654	.27327	.75	1.5119	3.2776	2.2776	1.1388	.95	3.2026	61.665	60.665	30.332